A generative learning model for saccade adaptation

Carlos R. Cassanello[1,2], Florian Ostendorf[3], and Martin Rolfs[1,2]

[1]Department of Psychology, and [2]Bernstein Center for Computational Neuroscience
Humboldt Universität zu Berlin, Philippstr. 13 Haus 6, 10115 Berlin, Germany
[3]Department of Neurology
Charité – University Medicine Berlin, Augustenburger Platz 1, 13355 Berlin, Germany

Running head: Generative learning model for saccadic adaptation

Key words: visually-guided saccades, sensorimotor learning, oculomotor plasticity, parameter estimation

Number of display items: 9 Figures and 2 Tables
Word count: 296 (Abstract) and 14856 (Body)

Corresponding authors:
Carlos R Cassanello (cassanec@hu-berlin.de) & Martin Rolfs (martin.rolfs@hu-berlin.de)

Abstract

Plasticity in the oculomotor system ensures that saccadic eye movements reliably meet their visual goals—to bring regions of interest into foveal, high-acuity vision. Here, we present a comprehensive description of sensorimotor learning in saccades. We induced continuous adaptation of saccade amplitudes using a double-step paradigm, in which participants saccade to a peripheral target stimulus, which then undergoes a surreptitious, intra-saccadic shift (ISS) as the eyes are in flight. In our experiments, the ISS followed a systematic variation, increasing or decreasing from one saccade to the next as a sinusoidal function of the trial number. Over a large range of frequencies, we confirm that adaptation gain shows (1) a periodic response, reflecting the frequency of the ISS with a delay of a number of trials, and (2) a simultaneous drift towards lower saccade gains. We then show that state-space-based linear time-invariant systems (LTIS) represent suitable generative models for this evolution of saccade gain over time. This *state-equation* algorithm computes the prediction of an internal (or hidden state-) variable by learning from recent feedback errors, and it can be compared to experimentally observed adaptation gain. The algorithm also includes a forgetting rate that quantifies per-trial leaks in the adaptation gain, as well as a systematic, non-error-based bias. Finally, we study how the parameters of the generative models depend on features of the ISS. Driven by a sinusoidal disturbance, the state-equation admits an exact analytical solution that expresses the parameters of the phenomenological description as functions of those of the generative model. Together with statistical model selection criteria, we use these correspondences to characterize and refine the structure of compatible state-equation models. We discuss the relation of these findings to established results and suggest that they may guide further design of experimental research across domains of sensorimotor adaptation.

Author Summary

Constant adjustments of saccade metrics maintain oculomotor accuracy under changing environments. This error-driven learning can be induced experimentally by manipulating the targeting error of eye movements. Here, we investigate oculomotor learning in healthy participants

in response to a sinusoidally evolving error. We then fit a class of generative models to the observed dynamics of oculomotor adaptation under this new learning regime. Formal model comparison suggests a richer model parameterization for such a sinusoidal error variation than proposed so far in the context of classical, step-like disturbances. We identify and fit the parameters of a generative model as underlying those of a phenomenological description of adaptation dynamics and provide an explicit link of this generative model to more established state equations for motor learning. The joint use of the sinusoidal adaption regime and consecutive model fit may provide a powerful approach to assess interindividual differences in adaptation across healthy individuals and to evaluate changes in learning dynamics in altered brain states, as sustained by injuries, diseases or simply aging.

Introduction

The accuracy of saccadic eye movement is maintained through mechanisms of saccade adaptation, which adjust the amplitude [1-3] or direction [4-6] of subsequent movements in response to targeting errors. As online visual feedback cannot be used to correct the ongoing movement, saccadic eye movements need to be preprogrammed and adaptation must largely rely on past experience and active predictions [7,8] rather than closed-loop sensory information.

To induce saccade adaptation in the laboratory [1], participants are instructed to follow a step of a target stimulus with their eyes and this visual cue is then displaced further during the saccade eye movement. Typically, this second, intra-saccadic step (ISS) is constant across trials and directed along the initial target vector towards smaller or larger saccade amplitudes. Although the ISS is visually imperceptible [9], saccades adjust their amplitude to compensate for the induced error. In phenomenological analyses of such saccade adaptation data, the amount of adaptation is usually quantified by comparing saccade gain values before and after the adapting block and interpolating an exponential fit in between [1-3,10].

We recently presented a version of this paradigm in which the ISS (the disturbance responsible for inducing adaptation) follows a sinusoidal variation as a function of trial number [11,12]; see also [4,13,14]. We reported that gain changes were well described by a parametric functional form consisting of two additive components. One component was a *periodic response* reflecting the frequency of the ISS that was adequately fitted with a lagged but otherwise undistorted sinusoid. The second component constituted a *drift of the baseline* toward lower saccade gain (larger hypometria) that was appropriately accounted for using an exponential dependence.

Here, we investigate whether a generative algorithm that models saccade gain modifications on a trial-by-trial basis by learning from errors made on previous trials can account for this response. To this end, we implemented and fit a series of state-space models in which a modified delta-rule algorithm updates a hidden or latent variable (for which the experimentally observed adaptation gain is a proxy) by weighting the last experienced visual error, in addition to other error-based and non-error based learning components [8,15-23].

We adopt the approach that these algorithms are linear time-invariant systems (LTIS), in that their coefficients are time and trial-independent. LTIS models, also known as linear dynamical systems (LDS) have been successfully used in a number of motor adaptation studies [8,19-22,24-27]. Applied to saccade adaptation, they may predict the dynamics of the saccade amplitude itself as well as various forms of movement gain typically used in describing adaptation [2,3,10,11]. Our first goal was to establish empirically whether LTIS models could fit the data recorded with a sinusoidal adaptation paradigm, as efficiently as when using a constant (fixed) ISS. Once we have established this point, we will explore the relation between the predicted phenomenological parameters [11,12] and the learning parameters of the underlying generative model, as well as their potential dependence on the perturbation dynamics.

We first analyze the ability of a family of generative models to describe experimental recordings of saccade adaptation by fitting the relevant learning parameters. We then perform statistical model-selection analysis to determine those that best fitted the same data. We fitted models to two data sets, a previously published one [11] and a variation of that paradigm that extended the range of frequencies. We then explore consequences for current models of motor learning and suggest possible modifications that may be required to generate a suitable description of sensorimotor learning during sinusoidal saccadic adaptation. In conducting this selection, we confirm that a single learning parameter model (a state-equation with just an error-based learning term; cf. [19]) does not suffice to fit the data. We then demonstrate that improvement in the fittings is achieved by including an extra term that weights the next-to-last trial's error. This learning rate has the intriguing feature that it has negative values for all frequencies, suggesting an active unlearning of the next-to-last trial's feedback error, close, but not equal in magnitude to the learning rate of the last trial's error. We discuss possible functional roles of these processes for oculomotor adaptation in natural situations, where saccadic accuracy is expected to exhibit slow dynamic changes across time.

Part of the material discussed in this contribution have been presented in the form of posters or slide presentations [28,29].

Materials and methods

Procedure

We re-analyzed the data we recently collected using a fast-paced saccade adaptation paradigm with a sinusoidal disturbance. We had previously described these data by fitting a phenomenological model that we identified using statistical model selection. For details on the experimental procedures pertaining to this original data set (henceforth, ORIG) and to the selection of the functional form of this phenomenological model, please refer to our former communication [11].

We applied the same experimental procedure in collecting further data with an enhanced range of frequencies. In this case, thirteen participants ran two sessions with similar Two-way and Global adaptation protocols as used in previous reports [11,12]. In short, Two-way adaptation refers to bidirectional adaptation along the saccade vector of saccades executed along the horizontal meridian. In turn, Global adaptation refers to adaptation along the saccade vector of saccades executed in random directions.

In collecting this dataset (henceforth, FREQ), each session had 2370 trials divided in 11 blocks. Odd numbered blocks had 75 no-adaptation trials (zero ISS). The five even-numbered blocks consisted of 384 trials each with a sinusoidal disturbance similar to that used before but with frequencies of 1, 3, 6, 12 and 24 cycles per block (i.e., 384, 128, 64, 32, and 16 saccades per cycle, respectively). The order of adaptation blocks was randomly interleaved for each observer and type of adaptation. The program was paused after each adaptation block, giving participants some resting time, and we calibrated eye position routinely at the beginning of each non-adapting (odd-numbered) block. In each trial, the pre-saccadic target step was fixed at 8 degrees of visual angle (dva). The subsequent second step (ISS) then ranged between –25% and +25% of the first step, changing size according to a sine function of trial number.

The Ethics Committee of the German Society for Psychology (DGPs) approved our protocols. We obtained written informed consent from all participants prior to their inclusion in the study. The present study conformed to the Declaration of Helsinki (2008).

Data analysis and phenomenological model

Modeling of the saccadic response. In a double-step adaptation paradigm [1], after a fixation interval the fixation target $FP(n)$ undergoes a first step to become the target of a saccade, displayed at the pre-saccadic location $TP1(n)$. Because the eyes might have been stationed at a location $EP1(n)$ close to but different than $FP(n)$, we define $TP1(n)$ with origin at $EP1(n)$ rather than $FP(n)$ and keep this convention throughout the study.

The second step of the McLaughlin paradigm (i.e., the target displacement inducing a feedback error) then shifts the target during the saccade ($ISS(n)$). Therefore, the post-saccadic position of the target (the target position at or immediately after saccade landing) $TP2(n)$, is given by the identity: $TP2(n) = TP1(n) + ISS(n)$. For convenience, we will define a *target gain*, $t(n)$, as the ratio of the post-saccadic target amplitude to the pre-saccadic one, as well as a *disturbance gain*, $d(n)$, as the ratio of the second to the first target steps, i.e., the ratio of the ISS to the saccade proxy:

$$t(n) = \frac{TP2(n)}{TP1(n)} = 1 + \frac{ISS(n)}{TP1(n)} = 1 + d(n). \tag{1}$$

In the general case, there would be a constant and a variable component in the second target step, $ISS(n) = C + V(n)$. In our sinusoidal adaptation paradigms, $C = 0$ and $V(n) = P\sin\left(\frac{2\pi f}{N}n\right)$ is a sine function of the trial number so that:

$$t(n) = 1 + \frac{ISS(n)}{TP1(n)} = 1 + c + v(n) = 1 + p(n) \cdot \sin\left(\frac{2\pi f}{N}n\right), \tag{2}$$

where c and $v(n)$ are the ratios of the constant and variable part of the ISS to the pre-saccadic target amplitude. In the sinusoidal paradigms, f is the frequency of the sinusoid in cycles per block, N is the number of trials in an adaptation block, and n is the index of the current trial. At fixed amplitude, the dynamics of the disturbance is fully determined by its angular frequency $\omega = \frac{2\pi f}{N}$, that characterizes the rate of change of the sinusoid in each trial. P is the maximum absolute magnitude of the variable part $V(n)$, i.e., the 'amplitude' of the sinusoid that defines the ISS. It was fixed at 2 dva throughout

all sinusoidal adaptation datasets. Therefore, $_{ISS}(_n)$ changed in magnitude periodically and in a sinusoidal fashion between –25% and +25% of the magnitude of the pre-saccadic target eccentricity ($_{TP1}(_n)$), which was held approximately fixed at 8 dva in all datasets. Finally, $_p(_n)$ is the ratio of *P* and $_{TP1}(_n)$, and had an approximately constant value of 0.25 across the sinusoidal datasets (the slight dependence on the trial number was a consequence of the slight dependence of the normalizing factor $_{TP1}(_n)$ on the trial number). Given that we used integer number of cycles across all sinusoidal adaptation experiments, we expressed the frequency in cycles per block (cpb). We set the initial phase to zero, which means that the magnitude of the ISS starts at zero in the direction of positive $_{ISS}$ (outward second-steps of the saccade target) first. **Equation 2** provides a complete description of the stimulus that we used. Yet, for the analyses pursued here and to make closer contact with our phenomenological characterization of oculomotor responses in sinusoidal adaptation [11], we will further define a *stimulus gain,* $_s(_n)$, to be the disturbance gain normalized to (i.e., divided by) its maximum absolute value. Therefore, $_s(_n)$ would range within $_{\pm 1}$ in units of its maximum amplitude following a sinusoidal variation with trial number:

$$s(n) = \left|\frac{TP1(n)}{\|ISS\|}\right|\left(\frac{TP2(n)}{TP1(n)} - 1\right) = \frac{ISS(n)}{\|ISS\|} = \frac{1}{\|d\|}d(n) = \sin\left(\frac{2\pi f}{N}n\right). \quad (3)$$

Saccade amplitude adaptation is usually described in terms of the changes in *saccade gain* ($_{SG}(_n)$), defined as the ratio of the saccade amplitude ($_{SA}(_n)$) to the pre-saccadic position error ($_{TP1}(_n)$, measured from the eye position at saccade onset as explained above). During non-adapting trials and at the beginning of the adaptation blocks, $_{SG}(_n)$ is typically slightly smaller than 1, which means that the saccade undershoots the target. Since we are interested in keeping track of the excursions of the saccade gain with respect to a perfect completion of the saccade that matches $_{TP1}(_n)$ exactly, we shall define an *adaptation gain* subtracting one from the usual saccade gain and normalized to the maximum absolute value of the $_{ISS}$,

$$g(n) = \frac{TP1(n)}{\|ISS\|}(SG(n) - 1) = \frac{SA(n) - TP1(n)}{\|ISS\|}. \quad (3a)$$

The adaptation gain represents the residual of the saccade gain with respect to perfect landing. When a saccade lands exactly on the first target step (a perfectly accurate saccade), the saccade gain will be one while the adaptation gain will be zero. Therefore, the adaptation gain uses perfect landing as the origin of coordinates and quantifies departures from this ideal goal state. Clearly, in both descriptions the reference represents a state of no adaptation. The adaptation gain description may be viewed as following the evolution of the error rather than that of the full eye movement. As long as the true underlying learning model is strictly linear, both descriptions must be equivalent since they relate to each other by a shift. We used the adaptation gain, $_{g}(_{n})$, in our previous reports [11,12] to provide phenomenological parametric description of sinusoidal adaptation data and it is also commonly used within motor control research. Throughout the manuscript we shall use $_{SG}(_{n})$ or $_{g}(_{n})$ as the relevant behavioral (experimentally extracted) variables describing the data, which are computed directly from the experimental measurements of the eye and target positions in each trial.

Estimation of the parameters of the phenomenological description of the behavior. To estimate parameters of the phenomenological functional form that best fits the data we used the same general procedure and the same parameter estimation algorithm implemented in our earlier contribution [11,13].

Assessment of the evidence in favor of a model. In implementing the phenomenological parameter estimation, we adopted a Gaussian likelihood for the data given the model. This likelihood can be maximized with respect to the parameters at a fixed but unknown width. Instead we adopted the following procedure [11,13]. Using Bayes theorem, priors for the parameters to be estimated, and assuming a constant prior probability for the data, we can obtain a joint probability amplitude for all parameters that can be marginalized to extract individual probability amplitudes for each parameter. In this process, the width of the Gaussian likelihood is a nuisance parameter that we integrate out using a non-informative prior [13,30,31]. Once such integration is conducted, the volume of the resulting probability density (given the data) provides an estimate of the odds that the model would provide a reasonable description of the data. Here we provide a full model consisting of six

190 parameters (sinusoidal entraining of the oculomotor response riding over a baseline drift) that we
191 want to compare to a partial model (the drift of the baseline alone) and to a minimal model consisting
192 of the mean of the adapting block with variance equal to the variance of the recorded data over that
193 block. To establish which situation is more likely across different number of parameters, we take the
194 log of the ratio of the odds across the models. The resulting magnitude is the *evidence* that the data
195 are in favor of a particular model and is measured in *decibels* (db). When this magnitude is positive,
196 the odds favor the model in the numerator, with evidence higher than 3 db indicating that this model
197 is significantly favored to the one in the denominator. We use this metric to assess the quality of our
198 parameter estimation.

199 *Statistics.* Throughout the manuscript we report results as mean ± SD for individual data and mean
200 ± SEM when we discuss group data. In the phenomenological fittings, to determine average
201 parameters from the parameter estimation other than the frequency, we computed the mean and
202 variance for each parameter and participant as the first two moments of the corresponding posterior
203 probability distribution and took the average of the means weighted by their standard deviations
204 (square root of the estimated variance) to generate each point on the population plot. Alternative
205 estimators (e.g., the modes of the posterior distributions, with and without weighting) gave
206 qualitatively similar results.

207 *Modeling of the sensorimotor learning process: the modified delta-rule state equation.*

208 To investigate generative models, we adopt the following rationale. In each trial, the oculomotor
209 system must generate a motor command to produce the impending saccade. This needs to be
210 calibrated against the actual physical size of the required movement [15,20,22,24,32,33].

211 If the saccade fails to land on target, the motor command needs to be recalibrated based on
212 preexisting calibrations, and we will hypothesize that those changes take place in an obligatory
213 manner (cf. [19]) through additive, error-based modifications attempting to ameliorate post-saccadic
214 mismatches between the eyes' landing position and target location.

We model the underlying sensorimotor learning using linear time-invariant systems (LTIS) because the model parameters (or the learning coefficients) are time independent in each experimental block, although they can vary across experimental conditions or phases [34]. These models are closely related to linear dynamical systems (LDS; cf. [20-22]), except that here we only address noise-free models.

Because saccades are extremely rapid movements that do not admit reprogramming in mid-flight, it is assumed that all gain changes take place in between saccades. In our models, therefore, the error-based correction terms weight errors that were experienced in previous saccades. As a consequence, in the estimation of the forthcoming event, the post-saccadic stimulus gain is not compared against the adaptation gain measured for that trial but against the previous estimate of the gain. To justify these assumptions, it is usually assumed that the motor system sends an *efference copy* of the motor command to the sensory areas, which enables prediction of the sensory consequences of the movement and therefore avails comparison to experienced post-saccadic feedback [7,19,20,33,35-37].

We will assume that the values of saccade and adaptation gains observed and extracted from the recorded data (i.e., $SG(n) = \frac{SA(n)}{TP1(n)}$ and $g(n) = \frac{SA(n) - TP1(n)}{\|ISS\|}$) are adequate proxies of that motor calibration process. Yet the calibration itself is an internal feature of the brain and therefore the *adaptation gain* that enters the generative algorithm (the state-equation) that we intend to study is a *hidden variable* representing the *internal state* of the system. A model providing its temporal evolution can then be fitted to the data; yet the variable itself is not experimentally accessible. We denote the internal variable associated to the saccade gain by $z(n)$. To describe the evolution of this *state* variable we introduce the state-equation:

$$z(n+1) = A \cdot z(n) + K \cdot \big(t(n) - z(n)\big) + M + D \cdot \big(t(n-1) - z(n-1)\big), \qquad (4)$$

supplemented with an initial condition that sets the initial value $z(1) = G \cdot t(1)$. Here, the target gain $t(n)$ is available from recordings in each trial and we shall assess how well the *prediction* of the saccade gain ($z(n+1)$, provided by **Equation 4**) fits the recorded data $SG(n)$. The first term on the

RHS of the equation is a persistence term. The persistence rate $_A$ determines how much of the estimate of the state variable at trial $_n$ is transferred to the estimate at the next trial [8,25,38]. Therefore, its magnitude is expected to be typically slightly smaller than 1 and it is set to be 1 in the models that do not include its effect. The second term weights the discrepancy between the gain of the target at trial $_n$ and the predicted gain of the movement under the underlying assumption that the size of the state variable is an adequate proxy for the (sensory) consequences of the movement. The weighting coefficient $_K$ is called *learning rate*. $_M$ embodies any systematic effect (drift or bias) that takes place in each trial but is not directly determined by the sensory feedback 2[39]; we shall call it a drift parameter. The last term is a second error-based correction term that weights the discrepancy between the gain of the target and the estimate of the movement at a trial other than the last error with and additional (distal) learning rate $_D$. For concreteness we shall assume that this correction is based on the sensory feedback arising from the next-to-last trial. However, we shall return to this specific assumption further in the **Discussion**. Note that with the inclusion of this hypothetical double error-sampling the full model of **Equation 4** (and **Equation 5** below) becomes an algorithm that coherently uses a doubly-delayed feedback to estimate the state of a single internal variable that models the sensory consequences of the intended motion.

Formatting of the data for fittings of the learning model. To be able to consistently compare results from this manuscript with the phenomenological analyses of the data presented in our earlier report, we will write the generative model in terms of a state variable associated to the *adaptation gain* of **Equation 3a** (cf. [11], and therefore naturally defined as $_x(n) = \frac{1}{p}(_z(_n) - 1)$. Applying these changes, we obtain:

$$x(n+1) = A \cdot x(n) + K \cdot (s(n) - x(n)) + m + D \cdot (s(n-1) - x(n-1)). \quad (5)$$

As suggested by **Equations 4** and **5**, a sensorimotor learning model can be written in terms of hidden variables that would be naturally associated with the saccade gain or the adaptation gain defined in **Equations 3** and **3a** respectively. When transitioning from the saccade gain to the adaptation gain description in this linear model, the only parameter of **Equation 4** susceptible to changes is M, which

we indicated in **Equation 5** using the lower-case m instead. Throughout the manuscript we adopt the adaptation gain (defined above), as the state variable to characterize the internal model and **Equation 5** as its relevant state-equation. In this description, the stimulus gain reduces to a pure sinusoidal disturbance with zero mean (i.e., with no static component), which minimizes confounds between the effects of the retention rate A and the drift parameter m.

Because movement gains are computed from experimental observations, models of motor control often include a second equation that maps the estimates of the hypothesized internal variable to real-world observations (see, e.g., [21], [20]). In our simplified analyses and again invoking the pre-programmed nature and accuracy of saccades, we set this second (observation) stage to be an identity.

Estimation of the learning parameters, model classification and model selection.

We conducted our analyses using the full form of **Equation 5**. We were interested in determining which model suffices to account for the data with the least number of parameters. The magnitude being learned is x, the internal representation of the adaptation gain of the imminent saccade. This gain has value zero upon the ideal outcome of perfect movement accuracy and in that respect, it can be interpreted as the gain of an internal prediction error. Using **Equation 5**, we generated the predicted values of $x(n)$ in each condition and for each participant, and then fitted a number of models that differed from each other in which parameters were estimated. When a parameter among K, m, or D was not present, the corresponding term was removed from **Equation 5**. Note however, that when the parameter A was not included as a fitting parameter, its value was set to unity (i.e., $A = 1$). In the case of the initial value G, we obtained an estimate by taking the average of the first five valued of the gain. We proceeded in this way because the initial value of the state of the system is unknown and, while the first recorded value of the gain could be considered a proxy for such initial state, execution and motor errors could yield a value of the gain significantly different than the actual initial state of the system; we averaged over 5 trials to alleviate this problem. In models where the initial value of the gain was left free to become a fitting parameter, this average over the first five saccades was used as an initial value for the fitting routine for that particular parameter.

Improvements can be achieved by letting the initial condition become an extra parameter. We discuss below the interpretation of using the initial condition as a fitting parameter of the model.

In view of these features of the generative model, a natural classification of the models tested arises as follows: given the parameters $K] \, A, m, D_1, \cdots, D_w \, [\, G$, we will 1) include K in every model because we are modeling intrinsic learning where we assume that learning from the last experienced feedback is always present as well as obligatory [19,20,22,33]; 2) models will be generated by adding successively the parameters A, m, and D, of which one or more could be present but in this study we restrict ourselves to learning possibly from only one extra feedback in the past; 3) G is an optional parameter that is included in an attempt to alleviate extreme effects of the initial condition(s) as explained above. By applying points 1) through 3), sixteen different models can be generated. For reasons to become clear below we would group them in four families according to whether or not they contain the bias term (m) and the additional error term (with learning rate D): K only (although with $A = 1$ when omitted), KA, KG, KAG feature zero bias and a single error term; Km, KAm, KmG, $KAmG$ are models with a single error term that allow bias; KD, KAD, KDG, $KADG$ have no bias term but sample two errors, and KmD, $KAmD$, KmDG, $KAmDG$ feature both a bias term and learn based on double error sampling. Therefore, the simplest model had a single fitting parameter (the learning rate K, cf. [19]) and was obtained by setting $A = 1$, removing the terms that involved m and D, and setting the initial value G to be the mean of the first five values of the gain in the block. The full model had all five as fitting parameters.

All parameters of the generative models were estimated by fitting the model to the experimental data using MATLAB function nlinfit; 95% parameters confidence intervals were computed using MATLAB function nlparci and predicted response for the hidden variable x with its corresponding 95% confidence intervals were obtained from MATLAB function nlpredci.

All 16 models were fitted to each individual participants' data, parameters were extracted for each model, then models were compared using the Akaike information criterion (AIC; [40-43]) by computing Akaike weights across models for each participant. Finally, these weights were averaged

across participants for each model and further compared to similar weights obtained from group data.

Using the generative model to predict the parameters of the phenomenological description of the adaptation gain

The adaptation gain of the oculomotor response to a sinusoidal disturbance is best described by a phenomenological function consisting of a decaying exponential added to a lagged but otherwise undistorted sinusoid [11]. The sinusoidal component of the response onsets at the beginning of the adaptation block but all fittings include the pre-adaptation block as well. The frequency of the stimulus disturbance is matched closely by the gain. To fully describe the response, five extra phenomenological parameters are required: amplitude (a) and lag (ϕ) of the periodic part of the error gain complete the description of the periodic part. The exponential decaying component that describes the baseline on which the periodic response rides requires other three: an asymptotic value (B_0) where the baseline stabilizes at large trial number, a timescale (λ) in which the baseline reaches $1/e$ of the full decay, and the amplitude of the decay (B):

$$g(n) = a \cdot \sin(\omega n - \phi) + Be^{-\lambda n} + B_0, \qquad \text{with} \qquad \omega = \frac{2\pi\nu}{N}. \tag{8}$$

We use here the same denominations used in our previous report [11], except for changing the name of the timescale to λ to prevent confusion with the amplitude of the periodic component a. Solving the state-equation via iteration in the simpler case where the system learns only from the last experienced feedback (cf. **Appendix A**), or borrowing techniques from the theory of LTIS reveals a correspondence between these phenomenological parameters and the coefficients of the generative model of **Equation 5**. (In a separate contribution, we shall provide a complete derivation of the phenomenological parameters as functions of those of the state-equation; details about the analytical procedures adopted can be found in [44]). Depending on the parameters that each generative model includes, the functional form and value of the phenomenological coefficients may change. Here we are interested in assessing which theoretical prediction of the relation among phenomenological and

generative model parameters matches the data best as a way to validate the underlying sensorimotor learning algorithm.

Lag and amplitude of the periodic response

The lag of the periodic response of the error gain derived from the (full version of the) generative model of **Equation 5** including the next-to-last feedback-error term is given by:

$$\begin{aligned} \cos(\phi) &= \frac{\cos\omega - (A - K - D\cos\omega)}{\sqrt{[\cos\omega - (A - K - D\cos\omega)]^2 + [(1-D)\sin\omega]^2}} \\ \sin(\phi) &= \frac{(1-D)\sin\omega}{\sqrt{[\cos\omega - (A - K - D\cos\omega)]^2 + [(1-D)\sin\omega]^2}} \end{aligned}. \tag{9}$$

In models without next-to-last feedback term D should be set to zero; in models that do not have A as a fitting parameter, its value should be set to 1 in **Equation 9**.

The periodic component of the response to a sinusoidal disturbance in models where the next-to-last feedback is included can be written as:

$$h(n) = \frac{K}{R}\sin(\omega n - \phi) + \frac{D}{R}\sin(\omega(n-1) - \phi), \tag{10}$$

where $R = \sqrt{[\cos\omega - (A - K - D\cos\omega)]^2 + [(1-D)\sin\omega]^2}$.

Equation 10 shows that if $D = 0$ we recover the solution expected by iteration when there is learning from the last error only. Then the amplitude of the periodic component (a) in **Equation 8** can be read out directly to be $a = \frac{K}{R}$. When $D \neq 0$ we need to re-write **Equation 10** so that it matches the periodic part of **Equation 8**. After some algebra **Equation 10** can be recast as:

$$h(n) = \frac{Q}{R} \cdot \sin(\omega n - (\phi + \varphi)) \tag{11}$$

where

$$Q = \sqrt{(K + D\cos\omega)^2 + (D\sin\omega)^2}, \quad \cos\varphi = \frac{K + D\cos\omega}{Q}, \quad \sin\varphi = \frac{D\sin\omega}{Q}. \tag{12}$$

Equations 9 to **12** clarify the effect of the presence of the next-to-last error learning rate D. **Equation 9** shows how the *bare* lag ϕ changes when D is present. Yet, it would be incorrect to compare the fitted values of the phenomenological lag to **Equation 9**. The reason is that the second contribution in **Equation 10** modifies not only the amplitude of the periodic component to the new value $a = \frac{Q}{R}$, but it also adds the shift φ to the lag. Therefore, if there were also learning from the next-to-last error, the observed (behavioral) lag should be compared to $\phi + \varphi$.

Baseline drift parameters

Following a sinusoidal disturbance, the baseline of the error gain will approach an asymptote at large trial number that can be written as a function of parameters of **Equation 5** as (see also **Appendix A**):

$$B_0 = \frac{m}{1 - (A - (K + D))} \tag{13}$$

The timescale for the decay of the baseline is given by:

$$e^{-\alpha} = \frac{1}{2}\left\{(A - K) \pm \left[(A - K)^2 - 4D\right]^{\frac{1}{2}}\right\} \tag{14}$$

When $D = 0$ this expression becomes $(A - K)$ which is always positive and smaller than 1 if the learning rate $K < 1$ and $A \sim 1$, therefore $\alpha = -\log(A - K)$ would be a positive and small number. Its inverse gives the number of trials that it takes for the baseline to decay to a level of $1/e$ of the size of the full decay. Therefore, we have four phenomenological parameters from **Equation 8**: B_0, λ, a, and ϕ. The former two parameters are already familiar from phenomenological descriptions of data in paradigms using fixed-sized second-step for the target. The latter are new, arising in paradigms with sinusoidal disturbances.

The amplitude of the decay of the baseline also bears dependence on the learning rates as well as on the initial condition. Because of the strong influence of the initial condition on this parameter, we refrain from a comparison of the behavioral fittings to the predictions from the generative model for this case.

Results

Analysis of the data at the phenomenological level

To obtain a general idea of patterns present in the data, we first collapsed the data for each stimulus frequency and adaptation type across participants (group data). We fit these data using a piecewise continuous function given by the addition of a monotonic (exponential) decay of the baseline – spanning both pre-adaptation and adapting trials- and a periodic entraining of the oculomotor response to the sinusoidal stimulus that begins at the onset of the adaptation block. This choice was supported by the fact that we had confirmed using statistical model selection criteria (i.e., AIC and BIC, [40-43,45]) that this functional dependence was the best descriptor of the oculomotor response among the set of models tested in Cassanello et al. [11]. **Fig 1** shows the group data in each dataset, along with the fits resulting from the parameter estimation based on the phenomenological model of **Equation 8**. The same parameterization was used to fit each participant's run. **Figs 2** and **3** summarize the estimation of the phenomenological parameters entering **Equation 8**. **Fig 2** shows the values of mean ± SEM of the parameters estimated from every individual dataset for each frequency and adaptation type that will be considered in further analyses.

Fig 1. Fits of the phenomenological model to the experimental data. The plots show adaptation gain (colored lines) averaged over individuals in the (**a**) Two-way adaptation and (**b**) Global adaptation condition of the ORIG data set (reported in [11]), as well as the (**c**) Two-way adaptation and (**d**) Global adaptation condition of the FREQ data set, using the same paradigm over an extended range of frequencies. The fit (black line) is based on **Equation 8**. The same equation was fitted to data from each participant in each condition and experiment, to estimate phenomenological parameters on an individual bases. For illustration purposes only, the figure depicts fittings done over the averages along with 95% confidence intervals (gray shaded areas).

Fig 2. Phenomenological parameters as a function of ISS frequency, estimated from both datasets (ORIG, diamonds, and FREQ, circles). (**a**,**b**) Amplitude (**a**) and Lag (**b**) parameters of the periodic (sinusoidal) component of the response. (**c**,**d**) Asymptote (**c**) and timescale (**d**) parameters of the monotonic drift of the baseline toward greater hypometria. Each point is a condition defined by type of adaptation and ISS frequency. Blue and red colors correspond to horizontal Two-way and Global adaptation, respectively. Error bars are SEM across participants. These four parameters are further compared to the values predicted by the solution to the generative models tested.

Fig 3. Assessment of the quality of the fits of the parametric phenomenological model to the group data. (**a**,**c**) Each bar is split into the log of the odds ratio of the full model to a drift only model that lacks the sinusoidal component (darker tone of the bars) added to the log of the odds ratio of the drift only model to the noise only model described above (lighter tone of the bars). For all but one condition (Global adaptation, 24 cpd), the full model provides the best account of the data. (**b**,**d**) Estimates of the frequency of the periodic component of the oculomotor response, for dataset ORIG (**b**) and dataset FREQ (**d**). Error bars are SEM.

Some features are readily apparent from these plots. First, the frequency of the ISS is reliably estimated (cf. **Fig 3b**,**d**). Second, the amplitude and the lag of the periodic components of the adaptation gain decay with increasing frequency of the stimulus (**Fig 2a**,**b**). The amplitudes of the periodic component are systematically larger in Two-way adaptation, while the lags observed in global adaptation are systematically larger than in the Two-way case. The systematic decay of the values of the lag with increasing frequency does not seem to extend to the smallest frequency (1 cpb in the new dataset). This may be related to the fact that at such low frequency the stimulus resembles more the behavior of a ramp that then turns rather than a truly periodic disturbance.

The parameters that affect the observed drift in the baseline (i.e., asymptote and timescale, **Fig 2c**,**d**) remain rather independent of the experimental condition. This feature is more apparent in the ORIG dataset, but it still seems to hold in the FREQ dataset. An exception arises at the lower frequency (1 cpb) tested in the FREQ dataset. However, the case of frequency one is rather special and should possibly be considered as transitional between periodic and non-periodic stimuli.

Fig 3 provides an idea of the quality of the fits by showing the *evidence* of the data in favor of the models tested (cf. [11,13,30]). Upper and lower rows correspond to Two-way and Global adaptation type respectively. For dataset ORIG, **Fig 3a** shows the logs of the odds ratio of the parametric model of **Equation 8** against a noise only model consisting of the block mean with variance similar to that of the data. Each bar is split into the log of the odds ratio of the full model to a drift only model that lacks the sinusoidal component (darker tone of the bars) added to the log of the odds ratio of the drift only model to the noise only model described above (lighter tone of the bars). This separation is possible because the models are nested so that the simpler models can be obtained from the full model by eliminating parameters. The evidence then compares the density of models likely to fit the data. **Fig 3b** shows the estimation of the frequency of the oculomotor response against the actual frequency of the stimulus for the three frequency values tested in dataset ORIG (3, 4, and 6 cpb). **Fig 3c** and **3d** shows the evidence and the agreement of the response with the five frequencies used in dataset FREQ (1, 3, 6, 12, and 24 cpb).

State-equation fittings and model selection

To assess the generative model, we fit **Equation 5** to all data available. We first show that the model provides a reasonable overall fit to the group data. **Fig 4** shows fits of the oculomotor response predicted by the full form of the generative model given by **Equation 5** with all five parameters described in the Methods section: $_{K}$, $_{A}$, $_{m}$, $_{D}$ as well as the initial condition $_{G}$. As before the qualitative agreement of the fits and the data is evident in both datasets. As we did in the case of the phenomenological fits, we included the pre-adaptation blocks in each condition in each dataset.

Fig 4. Fits of the oculomotor response predicted by the state-equation (Equation 5) with all five parameters. The plots show adaptation gain (colored lines), averaged over individuals in the (**a**) Two-way adaptation and (**b**) Global adaptation condition of the ORIG data set (reported in [11]), as well as the (**c**) Two-way adaptation and (**d**) Global adaptation condition of the FREQ data set, using the same paradigm over an extended range of frequencies. The stimuli input in the model fits is **s**(**n**) (cf. **Equations 1-3**), which is zero in the preadaptation block. The same equation was fitted to data from each participant in each condition and experiment, to estimate parameters of the generative model on an individual bases. For illustration purposes only, the figure depicts fittings done over the averages along with 95% confidence intervals (gray shaded areas).

We tested 16 different models that differed from each other depending on which parameters were fitted (see **Methods** for details). We then used Akaike's information criterion (AIC) to explore statistical selection among these models. Akaike weights (cf. section II of [42]) are shown in **Fig 5** segregated by model and condition for datasets ORIG and FREQ, respectively. In each condition (identified by adaptation type and stimulus frequency), we computed a matrix of weights in the following way. Because the best fitted model may differ between individuals, we first compute the AIC weights among the 16 models for each participant and condition. Then we averaged the resulting individual weights across participants. Results from this procedure are shown in **Fig 5**.

Fig 5. Akaike weights [42] for the 16 versions of the generative model, segregated by condition (frequency and type of adaptation). The label on the abscisa indicates the model for the weight displayed in the bars. The first three rows show results from dataset ORIG in the three frequencies for each type of adaptation (blue tones for Two-way, red tones for Global) tested. The bottom five rows are data from set FREQ. Frequencies for the corresponding row are shown at the top of each subplot in the first column. The first column shows the Akaike weights resulting from fitting the models to the group; the second and third columns are averages over participants of the individual weights for that model and condition. Vertical black dashed lines separate the four groups of models described in the subsection *Rationale for generative model building and parameter exploration* in the **Discussion** section (see text for further details).

Overall, two models appeared most suited to describe the oculomotor response obtained in the two datasets: The full model ($KAmDG$) and the model in which A was set to unity ($KmDG$). Indeed, these models outperformed the best models that included only a single learning rate (based on the last

experienced feedback), KAm and $KAmG$. In what follows, we will focus on a comparison of these four models.

Fig 6 shows the values of the generative parameters (Mean ± SEM, N = 10 for dataset ORIG, N = 13 for dataset FREQ) of the best models that learn only from the last experienced feedback error ($KAm, KAmG$). Upper and lower rows correspond to datasets ORIG and FREQ respectively. Learning rate K, persistence rate A and drift parameter m are shown in columns **a**, **b** and **c** of **Fig 6** respectively. **Fig 7** reports the parameters of the best models that update their hidden variable estimate based on a doubly delayed feedback (i.e., that learn from both last and next-to-last feedback error). Those models are $KmDG$ and $KAmDG$. **Fig 7 a-d** show respectively the learning rates K and D that weight the contributions of last and next-to-last feedback, the persistence rate A and the drift parameter m. Note that all models include the drift parameter m as a fitting parameter. We shall explain below why this should be expected.

Fig 6. Average over individual parameters of generative models $KAm, KAmG$, the best among those that learn from the last feedback only (cf. Equation 5 with $D = 0$). Blue and red colors correspond to horizontal Two-way and Global adaptation, respectively. (**a**) Learning rate K, (**b**) Persistence rate A, and (**c**) bias or drift-parameter m are plotted as a function of condition. Both favored models feature A and m as fitting parameters. Note the variability in their fitted values across conditions, in particular for dataset FREQ. Error bars are ±SEM.

Fig 7. Average over individual parameters of generative models $KmDG, KAmDG$, the best among those learning from last and next-to-last feedbacks (double error-sampling model; cf. full Equation 5). Blue and red colors correspond to horizontal Two-way and Global adaptation, respectively. (**a**) Learning rate K, (**b**) Learning rate D, (**c**) Persistence rate A, and (**d**) bias or drift-parameter m are plotted as a function of condition. Both favored models feature D and m as fitting parameters. Note that in both models, the bias parameter m, and the persistence rate A in model $KAmDG$, display much lower variability in their fitted values across conditions when compared to that of **Fig 6**. (**e**,**f**) Addition and difference of both learning rates, $\kappa = K + D$ and $\eta = K + D$ (see text for discussion).

Again, several features are readily apparent from these plots. The learning rates ($_K$ and $_D$) obtained from ORIG [11], show a rather clear segregation between Two-way adaptation and Global adaptation: $_K$ and $_D$ are larger for Two-way (blue colors) than for the Global case (red colors) suggesting that the extra variability brought upon by the random directions of the subsequent saccades characteristic of Global adaptation has a detrimental effect on all learning rates. They do not show a strong dependence on the frequency but the range of values used in that experiment

was rather narrow, ranging from 3 to 6 cpb. This segregation in the learning rates between Two-way and Global adaptation is also clearly present in the best models fitted to dataset FREQ.

A feature observed in all cases is that in models that learn only from the last experienced error, the (single) learning rate ($_K$) shows a mild increase with the frequency. This changes substantially if learning from the next-to-last feedback is included. In all of these models, the following features are observed. First, the magnitude of $_K$, the learning rate of the last-feedback error-correction term increases by about an order of magnitude with respect to the models that do not have next-to-last error-correction. Second, the magnitude of the next-to-last error learning rate ($_D$) is similar to that of the last error ($_K$) but with opposite sign. This seems to suggest that the next-to-last error is weighted negatively (or actively attempted to be forgotten) in the algorithm. Third, the discrepancy in magnitude between $_K$ and $_D$ is consistently larger for Two-way than for Global adaptation (compare the separation between corresponding blue and red lines in **Fig 7**, **a** and **b**). Fourth, the learning rate $_K$ reverses its dependence with the frequency of the stimulus with respect to the models without $_D$, and now decreases monotonically as the frequency of the stimulus increases. At the same time, the magnitude of $_D$ also decreases with the frequency. As a consequence, the discrepancy in magnitude between $_K$ and $_D$ is such that the addition of both learning rates approximately matches the range of the values of $_K$ fitted in the models that learn only from the last feedback (compare the values plotted in column **a** of **Fig 6** to those of column **e** in **Fig 7**). This suggests that when the additional error learning is not part of the model, the only learning rate fitted may represent an average across sub processes.

The values of the parameters fitted with the best four models are shown in **Supplementary Table 1** (Mean ± SEM, N = 10 for ORIG, N = 13 for FREQ). To assess dependence of the generative parameters on the experimental conditions we run 2 X 3 (ORIG) and 2 X 5 (FREQ) repeated-measures ANOVA on the fitted values using as regressors type of adaptation (Two-way and Global) and ISS frequency. Results are shown in **Supplementary Table 2** for the parameters given in **Supplementary Table 1**. We regard as more representative the results from dataset FREQ due to

the more extended range of frequencies tested. Consistent with the qualitative observations mentioned above, while type of adaptation is highly significant for the learning rates in every model, frequency show significance for $K$and D only in the models that feature double sampling ($KmDG$, for both datasets, $KAmDG$ only for FREQ) but not in those learning just from the last feedback ($KAm, KAmG$). As for the persistence rate, frequency is never significant suggesting that it can be kept fixed as in model $KmDG$. Type of adaptation is significant in KAm and $KAmG$ but such significance disappears in $KAmDG$.

Analytical solution of the generative model: predicting the phenomenological parameters: comparison to the group data

The iteration of state-equations that learn from the last feedback already qualitatively predicts both components of the phenomenological response. In general, the complete response can be interpreted as a convolution of the stimulus with a *response function*. This response function integrates the stimulus by weighting the disturbance over a temporal window, the size of which depends on the magnitude of the learning and persistence rates that combine to assemble the weights (cf. **Appendix A**). Contributions from constant components of the disturbance that arise either from constant features in the stimulus (as in the traditional fixed-ISS paradigm [1]) or from intrinsic biases that may not be strictly error-based in nature (e.g., in our case represented by the drift parameter; cf. [39]) accumulate across trials, changing saccade gain in a monotonic fashion akin to a drift of the baseline towards an asymptote. Iteration of the systematically varying part of the disturbance results in its convolution with similar weights but the trial-by-trial variation usually prevents finding a closed form for the series re-summation. For a sinusoidal disturbance, however, a closed analytical expression that describes this contribution in fact exists, it is periodic with the same frequency, lagging the stimulus by a number of trials. Two new phenomenological parameters of this periodic response—its amplitude and lag—bare characteristic dependences on the learning parameters.

Above, we fitted the extended version of **Equation 8** to the data and obtained and reported estimates for its phenomenological parameters (i.e., frequency $_{\nu}$, amplitude $_{a}$, lag $_{\phi}$, asymptote $_{B_0}$, timescale

λ and decay amplitude B; cf., **Fig 2** above). Similarly, we fitted the generative parameters for all generative models using the corresponding versions of **Equation 5**. **Figs 6** and **7** display those estimates for the four models that provided the best fits (excluding D: KAm and $KAmG$ and including D: $KAmDG$ and $KmDG$ respectively).

When there is a double sampling resulting in more than a single error-based term, **Equation 5** can be integrated using techniques standard within the theory of LTIS [44]. Based on these, we can derive analytical predictions of the phenomenological parameters as functions of the learning parameters fitted with the generative models (**Equations 9** through **14**). Here we attempt matching these predictions to the fitted values we obtained from the phenomenological parameter estimation implemented before (see **Fig 2**).

We start with **Equation 13** that provides a relationship between the expected asymptote of the adaptation gain at large trial number and the generative model parameters.

$$B_0 = \frac{m}{1 - (A - (K + D))}$$

A first significant observation about this expression is that in order to observe a drift in the baseline of the adaptation gain (i.e., in order to have an asymptote $B_0 \neq 0$), a finite value of the drift parameter m is strictly necessary. If m vanishes, the adaptation gain would maintain a baseline pinned at zero regardless of the values of K, A or D. In addition, in a situation where $A \sim 1$, $B_0 \approx \frac{m}{K + D}$ or $\frac{m}{K}$ in models where $D = 0$. Note that these are all signed magnitudes, not absolute values. In other words, a small learning rate K or a small number resulting from the addition $K + D$ will modulate the size of the asymptote and will determine its sign (i.e., will modify the degree of hypometria or hypermetria). Still a finite value for m is strictly needed to have non-zero asymptote. Recall that when m is not a fitting parameter, its value is set to zero. Due to the pervasive baseline drift across all of our data, all models favored under statistical model selection contain m as a fitting parameter, as pointed out above. Note, in addition, that the smaller the learning rate (K or $K + D$), the larger the size of the asymptote B_0.

Experimentally, we observed drifts towards higher hypometria in all averages and in most of the individual data. Note that formatting the data in terms of *adaptation gain* instead of *saccade gain* allows us to remove biases coming from constant contributions from the stimulus and therefore the parameter $_m$ should be regarded as intrinsic to the system. In other words, $_m$ characterizes or quantifies learning that would occur in absence of stimulus disturbance (i.e., with zero ISS), as if the system has an intrinsic propensity to modify its gain by virtue of environmental or experimental conditions not necessarily linked to an error.

In terms of the algorithms, the presence of finite m forces the selection of models that include $_m$ as a fitting parameter, which corroborates the results of the statistical model selection performed concurrently.

Fig 8a displays the matching of the analytical predictions of the asymptotes computed by inserting the fitted values of $_m$, $_A$, $_K$ and $_D$ into **Equation 13** for each participant's data, to the phenomenological estimation of $_{B_0}$ obtained from **Equation 8** and the parameter estimation of the phenomenological fits of the data for both datasets and both adaptation types.

Fig 8. Comparison of phenomenologically fitted parameters to their theoretical predictions based on the generative model. y-axes show the values obtained with the phenomenological parameter estimation (**Equation 8**); x-axes show predictions obtained by inserting the best estimated values of the generative parameters into the the analytical expressions of **Equation 9-14** (cf. '*Using the generative model to predict the parameters of the phenomenological description of the adaptation gain'* in the Methods section). Each row corresponds to one of the four best generative models. Each point is a single participant in a given condition and experiment. Data from the condition with a frequency of 1 cpb has been omitted because the predictions were poor for all models (in particular for the lag valiable, see the text for a discussion of this point). (**a**) Asymptotes of the gain at large trial numbers (**B_0** in **Equation 8** vs predictions by **Equation 13**). (**b**) Timescale of the decay of the baseline (**λ** in **Equation 8** vs predictions by **Equation 14**). Note the wide spread of the predicted values for models $\boldsymbol{KAm}$, and $\boldsymbol{KAmG}$ that also results in several ouliers beyond the limits of the subplot. In contrast, models $\boldsymbol{KmDG}$ tend to underestimate the phenomenological timescales. Model $\boldsymbol{KAmDG}$ provides the best prediction of the phenomenologically fitted values with only two points just beyond the limits of the plot. (**c**) Amplitude of the periodic component of the gain (**a** in **Equation 8** vs predictions by **Equations 10-12**). Note that models $\boldsymbol{KAm}$ and $\boldsymbol{KAmG}$ tend to underestimate the observed amplitudes of the peridic component of the gain. (**d**) Lag of the periodic component of the gain (**ϕ** in **Equation 8** vs predictions by **Equations 9-12**). The plots reveal a slight tendency for models $\boldsymbol{KAm}$ and $\boldsymbol{KAmG}$ to overestimate the length of the lag with respect to the predictions of the models including double error-sampling ($\boldsymbol{KmDG}$ and $\boldsymbol{KAmDG}$).

A second parameter commonly reported in saccade adaptation experiments and characteristic of the baseline drift is given by the timescale. **Fig 8b** shows the predicted values for the timescale resulted from inserting in **Equation 14** values of $_m$, $_A$, $_K$ and $_D$ fitted with the state-equation. There

is a clear overestimation of the baseline timescale in the models that do not feature double error sampling. As evident in the corresponding subplot, this is specially pervasive in the predictions arising from model KAm in the Two-way adaptation case where several individual data points fall outside the boundaries of the plot. Yet, models that include corrections based on the next-to-last error term seem to underestimate the timescale (in particular model $KmDG$).

Asymptote and timescale are parameters traditionally investigated and reported in adaptation to fixed-step disturbances. Sinusoidal adaptation paradigms provide two additional parameters associated to the periodic component of the adaptation gain observed in these protocols. **Fig 8c** and **d** compare predictions for the amplitude and the lag of the periodic component of the gain obtained by using **Equation 9** through **12** above. Data from both datasets suggest that models that do not feature double error sampling underestimate the magnitude of the amplitude of the periodic component of the oculomotor response (cf. predictions from these models in **Fig 8c**). This feature in fact is common to all models that learn from a single feedback and include $_{m}$ (besides models $_{KAm}$ and $_{KAmG}$; not shown) but the inclusion of D helps mitigating misestimation of this amplitude.

The last comparison is provided by the lag of the periodic component. **Fig 8d** compares predictions based on the state-equation learner (**Equations 9** and **11** furnish predictions for the components of the lag ϕ and φ after inserting the parameter values fitted with **Equation 5**) and the phenomenology (parameter ϕ in **Equation 8**). Arguably, **Fig 8c** and **d** are most informative in selecting which learning algorithm is better suited as an underlying predictor for the observed phenomenology. From them it is apparent that the models that include both $_{m}$ and $_{D}$ as fitting parameters provide better predictions, also displaying less variability across participants, in particular for the Two-way adaptation type. Among models with $_{D = 0}$, again models $_{KAm}$ and $_{KAmG}$ fit best. **Fig 8d** shows, however, that these models appear to overestimate the lag (cf. compare corresponding subplots in the figure), while models that have a second learning rate $_{D}$ match better the empirically observed lag. In addition, all models fail the estimation of the lag for a disturbance of frequency one as they all significantly overestimate the lag observed. Even though the predictions of the other phenomenological parameters are reasonable (the amplitude of the periodic component, timescale and asymptote),

predictions for the 1cpb condition for both Two-way and Global adaptation have been omitted altogether in **Fig 8**. This mismatch between the direct phenomenological estimation of the lag from the data and the analytical predictions arising from the integration of the state-equation for the case of the 1cpb condition, may be rooted in the fact that the functional dependence of the phenomenological parameters on the generative ones is determined by the specific sinusoidal dynamics of the driving stimulus, while the case of a 1-cpb frequency is the least periodic condition among all tested.

Discussion

We used a modified version of the traditional two-step saccade adaptation paradigm [1]; see [2,46] for reviews) in which the size of the second step varied as a sinusoidal function of trial number with an amplitude of 25% of a fixed pre-saccadic target amplitude. We recorded observers' eye movements at a total of six different frequencies and applied the sinusoidal disturbance always along the saccade vector which was aligned either in a horizontal bi-directional fashion (Two-way adaptation) or in random directions drawn from a uniform circular distribution (Global adaptation). The oculomotor response, quantified by the adaptation gain, followed the disturbance variation with comparable frequency, an amplitude ranging between 10 and 30% of that of the stimulus (i.e., 2.5 to 7.5% of the saccade amplitude), and lagging the stimulus by a few trials. In addition, it developed a systematic drift of the baseline towards larger hypometria that reached asymptotes of around 40% of the disturbance amplitude (i.e., 10% of the saccade amplitude) and was largely comparable across conditions. The phenomenological description in **Equation 8**—composed of a periodic response and an exponential decay—captured this behavior well and we estimated all six parameters pertaining to that description.

Rationale for generative model building and parameter exploration

In mathematical terms, the functional form in **Equation 8** is the integral solution of a family of LTISs of which **Equation 5** is a particular example. It is referred to as a state-equation or state-space model

because the internal variable x characterizes the gain or state of adaptation of the system. This algorithm is *generative* because it estimates the value of x at trial $n+1$ by modifying its estimate at the previous trial including possible effects of systematic biases and correcting the former value by weighting sensory feedback resulting from movement execution [21,26,47,48] (see also [25,34]; for further details on our specific use see the **Methods** section). Here we limit our discussion to *noise-free* generative models in that **Equation 5** does not include any noise term. Yet, **Fig 1** together with **Fig 4** suggest that integral solutions as well as numerical outcomes of noise-free generative models survive ensuing variability, at least for the paradigm, type of stimulus and within the ranges of the conditions tested.

We analyzed 16 models that differed in the specific parameters that were fitted and then used Akaike's information criteria to attempt model selection. Since we were primarily modeling intrinsic error-based sensorimotor learning, the learning rate K—that weights the impact of the last feedback error on the state of adaptation—was present in every model. Second, we included the initial condition G as a fitting parameter in half of the models. This parameter is not part of the trial-by-trial learning algorithm and its effect should decay as the trial number increases (cf., **Equation 7**). However, the initial condition affects the amplitude of decay of the baseline drift (cf. B in **Equation 8**). Because the argument of **Equation 5** is an internal variable not directly experimentally accessible, a proxy for its initial value can only be approximated (for example, by averaging the first five gain values in the block) or included as a fitting parameter. Third, we included a persistence rate A that weighted how much of the estimate from the previous movement remained in the subsequent one. In models that do not feature temporal decay of the internal state this rate was set to one. The fourth parameter, m, captured systematic effects, that are not error-based in nature, and gave origin to drifts in the baseline that were pervasive across all conditions. Finally, we considered the plausibility and study the effects of a second learning rate D that tracks errors other than the most recent (here, the next-to-last feedback error).

To further discuss the effect of the generative parameters, we split the 16 models into four groups:

I. Models that neither included terms depending on the second learning rate D nor the drift term m (K, KG, KA, KAG);

II. Models without terms depending on D but including m ($Km, KmG, KAm, KAmG$);

III. Models including terms depending on D but excluding m ($KD, KDG, KAD, KADG$);

IV. Models with both D and m terms included ($KmD, KAmD, KmDG, KAmDG$).

We recall that in models where A is not a fitting parameter, $A = 1$. The subplot in the upper right corner of **Fig 5** indicates the subdivision in four families mentioned above. Models within group I consistently fitted worst. Moreover, qualitatively speaking, in models that do not include m (groups I and III), the adaptation gain does not *saturate* or evolve into a stationary asymptotic value because the state equation does not admit a solution featuring that behavior (that is, if the stimulus has no constant term). These models, however, may be useful in experimental paradigms where a stable state of adaptation is not clearly reached either because the length of the adaptation block used may be too short or because the driving disturbance is unbounded (for example a linear ramp). On the other hand, models that include sampling from two errors (cf. groups III and IV) will likely be better suited to extract correlations built into the stimulus as it is the case of a sinusoidal ISS.

Given the variability in the AIC scores at the individual level, we guided ourselves in choosing the best models by assessing the group data first. This data is shown in the third column of **Fig 5**. The fits of the phenomenological model (**Equation 8**) to the group data (**Fig 1**) suggest that asymptotic behavior of the baseline and reflection of the stimulus self-correlation (entraining) were clear structural properties of the oculomotor response. The analytical solutions of models in both groups II and IV would be consistent with the phenomenology. Yet it remained to be decided whether corrections based on the memory of more than a single error was required. While models in group II already generated responses in qualitatively good agreement with the evolution of the adaptation gain, AIC scores over fits to the group data show that group IV clearly outperforms all others except for frequency 1cpb of the Global adaptation type, suggesting that the best generative model may include all four parameters K, A, m and D. In inspecting the actual values fitted across the population,

we also believe that the parameters A and m may be safely set to constant values, almost one for the former and very small and negative for the latter (cf. **Fig 7**, columns **c** and **d**), at least within the range of frequencies tested in these experiments.

Model comparison showed that a state-equation including a single parameter or any combination of only two of the four parameters K, A, m and D could not adequately account for our data (cf. **Fig 5**). More competitive models featured three or more parameters and the full model with A set to 1 (i.e., $KmDG$) yielded the best fits across both individual and group-level analysis. The drift parameter m and the second learning rate D proved useful and necessary to account for systematic effects in our data, suggesting (1) that some changes in the adaptation state are not error-based and (2) that—at least under specific circumstances—the brain keeps track of at least one extra occurrence of the error besides the last experienced one.

Drift in the baseline and the meaning of m

The persistent drift of the baseline towards higher hypometria is a distinctive feature in our data that cannot be accounted for on the basis of motor adaptation [49]. We included an extra parameter $_m$ to account for this drift in mean adaptation gain towards an asymptote differing from the mean of the stimulus (cf. **Equation 13**). Because in our paradigm the goal of the task was to land on the target as close as possible, and because the sinusoidal ISS introduced a continuously changing prediction error, the best expected outcome would be to track the disturbance within the levels of error typical of trials without disturbance. With respect to that goal, the presence of a baseline drift introduces an additional discrepancy that does not, however, hinder successful adaptation to the disturbance.

Saccadic eye movements slightly undershoot their target on average [50] and this systematic offset corresponds to the internally predicted visual outcome of a saccadic eye movement [51,52]. We surmise that our paradigm may have yielded a re-calibration of this desired offset [53] over the course of an experimental run. This recalibration towards a larger undershoot may result from the high probability of a quick return saccade after every eye movement in our fast-pace paradigm, reducing the utility of maintaining a saccade gain close to one. We note that this systematic decrease in

755 saccade gain may in general—albeit to different degrees—pervade the study of saccadic adaptation

756 (but see [7,54]). In fixed-step paradigms (as opposed to the sinusoidal paradigm employed here),
757 however, it would have been obscured as the error-based correction for the surreptitious target
758 displacement undergoes similar dynamics as the drift reported here.

759 On the other hand, from the point of view of the internal model of the movement that the brain may
760 implement [35-37], this bias parameter m may hint to a discrepancy between the experimental
761 coordinate system where measurements are acquired and the coordinate system in which the
762 internal model is represented.

763 The presence of a small and negative bias parameter indicates an asymmetry between inward and
764 outward adaptation. On a neurophysiological level, such asymmetry could be related to the dynamics
765 of complex spikes (CS) in the cerebellum, which are assumed to encode error (Reza Shadmehr,
766 *personal communication*, July 12, 2018). Briefly, the onset of the saccade target would already elicit
767 the production of a CS by the cerebellar Purkinje CS-On neurons encoding the specific saccade
768 vector. Because we always displaced the target along the direction of the saccade vector, the
769 subsequent error resulting from the ISS will either be in the preferred direction of the CS-on cells
770 that just fired (for positive, outward ISS), reducing its likelihood to fire again, or in the opposite
771 direction (for negative, inward ISS). As a consequence, adaptation would be more efficient for inward
772 than outward ISS. The fast-pacing used in our paradigm may exacerbate this asymmetry even in
773 absence of a sizeable ISS as the evolution of the baseline that we observed seemed to onset already
774 at the pre-adaptation block. This explanation further suggests that the magnitude of m may depend
775 on the inter-saccade interval as well as on the precise timing of the ISS onset. These possibilities
776 will be addressed in future studies.

777 *Consequences of learning from double error sampling (D parameter): Two learners?*

778 The models that best explained the data featured a double error sampling, learning not only from the
779 feedback experienced after the last saccade but also from the movement that occurred in a trial
780 before that. Hence, the best models used a doubly-delayed feedback through the K- and D-terms of

Equation 5. Yet, does the oculomotor system actually implement this double error sampling that may coherently participate in a single internal model prediction? We suggest that the brain may attempt to approximate the performance achieved by the double-error-sampling algorithm by using two single-feedback learners operating on appropriate combinations of the stimulus sampled at two different times.

To understand that, we return to **Equation 5**. For simplicity, we will assume that $m = 0$.

$$x(n+1) = (A-K)x(n) - Dx(n-1) + Ks(n) + Ds(n-1), \tag{5a}$$

and write a transformation among state variables sampled at two different trials as,

$$X_+(n) = \frac{1}{2}\{x(n) + x(n-1)\} \text{ and } X_-(n) = \frac{1}{2}\{x(n) - x(n-1)\},$$

that can be substituted in the RHS of **Equation 5a** using the inverse relations:

$$x(n) = X_+(n) + X_-(n), \text{ and } x(n-1) = X_+(n) - X_-(n).$$

We can re-write **Equation 5a** in terms of these alternative state variables X_+ and X_-:

$$X_+(n+1) + X_-(n+1) = (A-\kappa)X_+(n) + (A-\eta)X_-(n) + \kappa S_+(n) + \eta S_-(n),$$

(5b)

where we adopted the definitions of $\kappa = K + D$, $\eta = K - D$, $S_+(n) = \frac{1}{2}(s(n) + s(n-1))$ and $S_-(n) = \frac{1}{2}(s(n) - s(n-1))$. **Equation 5b** avails the interpretation of the generative model as selectively learning into two component channels that learn from a single feedback error taken from different sources. The source for the learner X_+ is the mean of the two samplings of the stimulus, i.e., $S_+(n) = \frac{1}{2}(s(n) + s(n-1))$. The source for the second learner is the rate of change of the stimulus across the sampling events given by $S_-(n) = \frac{1}{2}(s(n) - s(n-1))$ which, when the samplings occur on successive trials, it could be interpreted as the discrete time derivative of the stimulus taking the elementary timestep as the (average) inter-trial interval.

Note that the representation in terms of these alternative internal variables would significantly alter the underlying structure of the noise-free learning model. But if we insist on keeping a close connection to the parameters extracted using the double-error-sampling algorithm, we would expect that the learning rate for learner X_+ would be the addition of the rates for the two errors, $_K = K + D$, while for learner X_- it would be $\eta = K - D$ (cf. **Fig 7**, columns **e** and **f**). In all our fittings using the double error sampling, K and D were very close in magnitude but carried opposite sign. Furthermore, $_K$ was small and similar in magnitude to the learning rate K obtained for models that learned only from the last error. Because D was negative, the learning rate η for the second learner became also positive but much larger than $_K$, in fact about an order of magnitude larger (**Fig 7**, columns **e** and **f**) effectively enhancing the overall gain of the process without driving the system unstable [55-57]. As a consequence, $(A - \kappa)$, which can be thought of as an *effective* A_+ will be much closer to unity than $A_- = (A - \eta)$. Therefore, X_+ will learn and forget much slower than X_-.

Using this double error sampling, the oculomotor system could track the rate of change of the stimulus from one saccade to the next, besides just its last change in size and it would approximate the learning efficiency of the doubly-delayed algorithm. The new internal learning variables (X_+ and X_-) would learn from smoothed-out versions of the disturbance resulting from the average sum and difference of the two sampled inputs. Whether this constitutes an advantage over learning exclusively from the last feedback depends on the nature of stimulus. If the disturbance is constant or fully random there would be very little advantage in performing the double sampling. In the former case, the inter-sampling variation is zero leaving nothing to learn. In the latter, the inter-sampling variation would be another random magnitude and there would be little advantage in learning from the variation in the feedback. However, if the mean of the disturbance varies in a systematic way—as it does during sinusoidal adaptation, and presumably in natural scenarios—learning from its rate of variation would be advantageous and could well justify a large learning rate. In the representation of the double-error-sampling model, unlearning actively the next-to-last sampled feedback error (i.e., with a large and negative D subtracted from an enhanced K) would materialize this advantage with little extra investment. However, a negative learning rate feels counter-intuitive as learning is believed to follow the direction of the correction suggested by the feedback. Segregation of the

831 learning underlying motor (or saccade) adaptation into two learners displaying similar characteristics
832 to those suggested here have indeed been proposed in other contexts [8,25,58,59]. The argument
833 presented above suggests a mechanistic way to construct a two-learner system, in which the
834 components X_+ and X_- can be considered statistics in counterphase. To approximate the double-
835 error-sampling learner, the system may hold in memory both samples, compute mean sum and
836 differences between the samples and implement two learners based on those statistics rather than
837 from bare values of errors or stimulus occurrences. To achieve that, the oculomotor system would
838 need to keep memory and weight prediction errors from a former time scale besides the last feedback
839 [60].

840 An important point to notice is that, even if there is double error sampling, it does not need to be
841 strictly the next-to-last error. It would be enough that the brain keeps a correlation of errors over two
842 different trials (cf. [61]) although it would be reasonable that they are spaced only by a short delay
843 [55]. This is a reasonable generalization since the inter-trial interval is rather arbitrarily set by the
844 pacing of the task that may or may not match a possible internal sampling frequency by the brain.
845 The frequency of the stimulus then determines to what degree differences in the stimulus can be
846 sampled, which may explain the dependence of the amplitude and lag of the periodic component of
847 the response with the frequency as well as the fact that the evidence for the full model seems to
848 peak at intermediate frequencies. In other words, it may be easier to learn at certain frequencies (for
849 a fixed amplitude) or at certain effective rates of change of the stimulus.

850 *Dependency of learning rate on perturbation dynamics: Linear but not strictly Time Invariant Systems*

851 We further explored whether the values of the generative parameters exhibited dependence on the
852 experimental condition, specifically with the type of adaptation and the frequency of the disturbance.
853 The parameters of our models remained time-invariant across pre-adaptation and adaptation blocks.
854 However, we did not rule out that these parameters may change with adaptation type and stimulus
855 frequency. In fact, LTIS models with parameters not strictly time-invariant have been invoked to
856 model (meta-learning in) savings in adaptation to visuomotor rotations [34]. Strict LTIS models with
857 two learners had been able to successfully account for savings in long-term saccade adaptation

858 [8,25,59,62]) but were not able to fit differences in the dynamics of the adaptation, extinction and re-
859 adaptation phases observed using counter-adaptation and wash-out paradigms in adaptation to
860 visuomotor rotations without letting the rates change across the phases [34].

861 We limit our discussion to the best four generative models selected in the **Results** section. In models
862 KAm and $KAmG$ (and in general in all models of groups I and II), the (only) learning rate K remained
863 relatively independent of, or exhibited a tendency to grow with, the frequency of the stimulus (**Fig**
864 **6a**). Learning rates for Two-way adaptation roughly ranged between 0.01 and 0.035 fraction of the
865 error across the frequencies tested. The same parameter in Global adaptation was smaller and
866 remained within the range 0.005 to 0.015 (cf. **Fig 6a** and **Table 1**). These observations were
867 confirmed by ANOVAs run on the fitted values of the parameter K in models KAm and $KAmG$ in that
868 type of adaptation was always a significant factor while ISS frequency never was (**Table 2**). These
869 values of K compare reasonably well with the magnitude of learning rates previously reported in the
870 literature (cf. [8,19]). The dependence of the learning rate on the frequency of the disturbance seems
871 in qualitative agreement with results from reaching experiments in which subjects learned to track a
872 target undergoing surreptitious displacement that followed a random walk [32,47]. Using a Kalman
873 filter to estimate corrections to the learning rate due to various types of variability Burge and
874 collaborators [32] argued that the learning rate increased as the drift of the walker increased. In the
875 sinusoidal adaptation paradigm where the amplitude of the sine function that produces the ISS is of
876 fixed amplitude, this situation occurs when the frequency increases because its size from one trial
877 to the next changes faster. However, this suggestion seems at odds with the intuition that a more
878 consistent stimulus should drive more efficient adaptation [63,64]. In particular, it has been reported
879 that a smooth gradual variation results in more efficient adaptation [3,65]. If this were the case and
880 reflected onto the model parameters, the learning rate should be higher for smaller frequencies.

881 However, the dependence of the learning rate(s) on the frequency described above changed rather
882 dramatically when double error sampling was included (cf. **Fig 7**, columns **a** and **b**). Interestingly, in
883 models that feature double error sampling, the learning rate of the most-recent error-term (K)
884 reversed its tendency and decreased as the frequency increases, achieving its highest values in the
885 conditions of lower frequency, this is, in situations where the stimulus displayed higher consistency.

Concurrently, the learning rate for the next-to-last feedback (D) achieved its most negative values at lower frequencies and grew less negative as the stimulus frequency increased. In the alternative scenario of two additive learners with single error correcting terms that learned respectively from the half-sum and the half-difference of the two sampled errors suggested in the previous sub-section, the learning rates κ and η also showed a distinct dependency on the ISS frequency. The *slow-learner* (with learning rate $_{\kappa}$) would only have corrected up to 1% of the average of the two errors sampled while the *fast-learner* (with rate η) would have produced corrections of up to 40% of the change experienced between the two sampled errors (cf. **Fig 7e** and **f**). Note that this massive change in the dependence of the learning rates on the frequency was a consequence of changing the hypothesized structure of the model and not of correcting the magnitude of the rates for effects of variability. Once again, ANOVAs confirmed that not only the type of adaptation but also the stimulus frequency had significant impact on the learning rates (K and D, as well as κ and η) in models $KmDG$ and $KAmDG$ as well as all models of group IV (cf. **Table 2**).

In contradistinction, the retention rate A (**Figs 6b** and **7c**) and the bias parameter m (**Figs 6c** and **7d**) remained relatively independent of the frequency under such changes, although their overall variability was clearly reduced in the models featuring double error-sampling (contrast the value ranges of m and A in **Fig 6**, against the corresponding ones in **Fig 7**, aside from model $KmDG$ in which $A = 1$; see also corresponding entries in **Table 1**). ANOVAs run over these parameters further confirmed non-significance of the frequency except for model $KmDG$ on m in dataset ORIG (**Table 2**). Type of adaptation occasionally modulates A in dataset FREQ in models with a single error term. Taken altogether these suggests that both A and m may be largely frequency independent and can be modeled as constant values maybe differing in value for Two-way and Global types.

In summary, introducing a second error term increased the magnitude of both learning rates (K and D) by an order of magnitude with opposing signs. The learning rates of these models showed a clear dependence on the frequency of the disturbance: higher stimulus consistency (i.e., lower stimulus frequencies) correlated with higher adaptation efficiency. At the same time, the inclusion of the double error sampling reduced variability in the estimates of the persistence rate A and the drift

913 parameter m, indicating that their estimates were not affected by the ISS frequency, and could thus
914 be set to appropriate constant values.

915 *Relation to previous work on sensorimotor control and adaptation*

916 Multiple distinct learning processes contribute to sensorimotor adaptation. Recent research
917 conducted primarily within adaptation to visuomotor rotations or in reaching movements, suggests
918 that adaptation can be decomposed into two fundamental processes that may operate in parallel:
919 one that would be responsible for implicit learning that progresses slowly and can be described
920 mechanistically by a state-equation [49]. This slow learning process is relatively stable over breaks,
921 takes place with automatic, reflex-like behavior and its properties tend to be sturdy and do not change
922 fast with recent experience. A second, parallel process, in turn, learns explicitly, is faster although it
923 may require longer reaction time and possibly voluntary behavior to be engaged. This faster process
924 would exhibit longer term memory of prior learning [66-69].

925 We believe that our paradigm taps only the first, implicit component. Yet, we suggest that our
926 analyses provide evidence for two separable subcomponents, although both would be intrinsic in
927 nature [58]. In fact, a key difference between our oculomotor learning and learning that occurs in
928 adaptation to visuomotor rotations and during reaching in force fields is that our participants were
929 primarily unaware of the inducing disturbance. In contrast, in the aforementioned paradigms,
930 participants immediately notice a disturbance even when they may not be fully aware of the exact
931 effect. In this sense, our paradigm could be considered qualitatively closer to that used by Cheng
932 and Sabes [22] who studied calibration of visually guided reaching in participants fully unaware of
933 the stimulus manipulation. Their paradigm used a random, time-varying sequence of feedback shifts.
934 They found that a linear dynamical system (LDS) with a single error term and trial-by-trial state
935 update for variability implemented with an estimation-maximization algorithm successfully described
936 mean reach point and the temporal correlation between reaching errors and visual shifts. They
937 further argued that the learning taking place under a random stimulus generalizes to a situation of
938 constant shifts in a block paradigm and, therefore, that adaptation dynamics does not rely on the
939 sequence (or correlation) of feedback shifts but can be generally described with the LDS model. In

contrast to random or block constant ISS, our paradigm featured a disturbance that was fully self-correlated since it followed a sine variation with the trial number. Therefore, it may prove advantageous for the oculomotor system to extract correlations embedded in the disturbance because they would help tracking the target. As pointed out, including double error sampling would serve this purpose.

We believe that the presence of a systematically varying disturbance enables a further decomposition of the implicit component of adaptation, perhaps into a primary one, that attempts to mitigate the end-point discrepancy regardless of self-correlations in the disturbance, and a second one that attempts to extract (and use) such correlations. It remains an open question how these putative subprocesses may map on distinct or overlapping anatomical structures, such as cerebellar cortices, deep cerebellar nuclei and extracerebellar structures [60,70-73].

A recent study suggested that learning in dynamic environments may be adequately modeled with an algorithm popular in industrial process control, the proportional-integral-derivative (PID) controller [74]. The algorithm generates a control signal adding three error-related contributions: a term proportional to the current error that resembles a usual delta-rule (the P-term), a term that integrates over a history of errors experienced before the current one, and a derivative term estimated from the difference between the last two errors. The model shares some features with ours, in particular that the learning rate for the next-to-last error needs to be negative to approximate the derivative term. The PID controller acts on the actual recorded errors (the equivalent of the visual errors observed after each saccade is executed) and contains no internal state estimation, whereas our model operates on an internal variable that contains the state estimation of the prediction error that would result from the movement execution. Our state variable in fact accumulates and retains a substantial portion of the history of previous error (the persistence term in **Equation 5**, see also the example given in **Appendix A**), which is updated on a trial-by-trial basis by the term proportional to the latest prediction error (the delta-rule term). The inclusion of an extra error in our state-equation (specifically that of the previous to last one) effectively brings into play a contribution similar to the derivative term of the PID model. In short, our D-term enables a systematic correction to the integral term (our A-term) that otherwise would be determined rigidly by the iteration of the equation. In that respect,

keeping track of former errors enables a structural correction that acts at a global level even when it is introduced on a trial-by-trial basis, lending both robustness and flexibility to the algorithm. Ritz and collaborators [74] further compared the performance of the PID model to a Kalman filter used to update a state variable in presence of noise applied on the single error structure of the usual delta-rule and found that the PID controller performs better. A further similarity with the aforementioned work lies in their observation that models with a derivative term are usually not readily selected under statistical model selection even when they may display significant improvement in the description of the behavior (see [74] for a longer discussion on this point).

Conclusions

Having adequate generative models that describe eye movements have been stressed before [75-80] as an important tool to assess, at the single patient level, a variety of movement abnormalities that have been identified as markers of neurological conditions or disorders at a group level. In this study, elaborating on the idea of tracking a memory of errors [60], we attempted to identify and constrain a relatively minimal set of requirements that would suffice to model saccade adaptation data collected under the paradigm and stimulus that we recently implemented [12,28,29] but that would also include previous accounts of the phenomenon under other known paradigms. While certainly many refinements are still due, we unveiled features of an algorithm that seems suitable to account for the sensorimotor learning observed in our data. We hope it can be generalized, extended and adapted for use in future research.

Acknowledgements

This research was supported by the Deutsche Forschungsgemeinschaft, DFG (grants RO 3579/2-1, RO 3579/3-1, and RO 3579/8-1). We thank Thérèse Collins and members of the Rolfs lab for insightful discussions and help with data collection.

Appendix A

Predictions of a state-equation with a single, most-recent error-based correction term.

Iteration of a $KAmG$ model. An idea of the nature of expected responses can be obtained by iteration of **Equation 5**. For simplicity, we drop the term involving the second-to-last error ($D = 0$) to obtain:

$$x(n+1) = \left[G(A-K)^n + \{1-(A-K)^n\}\frac{m}{1-(A-K)}\right] + K\sum_{i=1}^{n} v(i)(A-K)^{n-i}. \qquad (A1)$$

We have inserted **Equation 3** so that $v(i)$ represents the portion of $s(n)$ that depends on the trial number. For sinusoidal adaptation datasets, $v(i) = p(i) \cdot \sin\left(\frac{2\pi f}{\mathrm{N}} i\right)$. **Equation *A1*** can be split into two major contributions, one involving only constant features of the disturbance (terms inside the square brackets) and another accounting for the portions of the disturbance featuring systematic variation. This structure resembles closely the two components identified in our recent phenomenological study of sinusoidal adaptation data [11,12,28,29].

Baseline drift: What is m and why do we need it? The first term of **Equation *A1*** describes a decaying drift similar to what we observed in the data. To understand better its evolution with the trial number, it can be rewritten as:

$$b(n+1) = \frac{m}{1-(A-K)} + \left[G - \frac{m}{1-(A-K)}\right](A-K)^n \qquad (A2)$$

The first term of **Equation *A2*** is independent of n and therefore represents an asymptotic value once all dependence on the trial number had subsided. The second term will decay as the trial number progresses as long as $(A-K) < 1$, which is the case in all data analyzed. If the first saccade undershoots the target, then $G = 1 - \delta$ and the factor in brackets in the second term becomes $1 - \frac{m}{1-(A-K)} - \delta$.

The simplest state-equation (cf. [19]) is recovered when $A = 1$, and $m = 0$. In that case the asymptote for our adaptation gain vanishes and one would expect the baseline to remain unchanged. However, we observed a pervasive drift towards higher hypometria across all conditions in the majority of the participants. This inward drift of the baseline can be modeled assuming that $m < 0$,

which could be interpreted as a systematic tendency to undershoot. As mentioned above, the sinusoidal stimulus does not contain any constant part because the disturbance is fully sinusoidal and centered at zero mean. Therefore, m is required to model the drift that we observed in the adaptation gain.

This is not the only reason why the simplest version of the state equation needs to be modified. Already in the case of a disturbance that only includes a constant part c (of positive or negative sign for outward or inward adaptation respectively), **Equation *A2*** will acquire an extra term proportional to that constant part, weighted by the learning rate K:

$$b(n+1) = \frac{m}{1-(A-K)} + \left[G - \frac{m}{1-(A-K)}\right](A-K)^n + \frac{K}{1-(A-K)}c\left[1-(A-K)^n\right] \qquad (A3)$$

Under the simplest state-equation ($m = 0, A = 1$) all that remains from **Equation *A3*** is $b(n+1) = c\left[1-(1-K)^n\right]$. Therefore, the asymptote would become c predicting fully complete adaptation, which is not typically observed in paradigms that employ fixed-size or random disturbances (Herman et al. 2013). The presence of m would prevent full adaptation. Lack of full completeness of adaptation could also be a consequence of a retention parameter $A < 1$. However, because the disturbance that we used did not have a constant component, even if $A < 1$, the model will not produce any drift of the baseline (cf. **Equations *A2*** and ***A3***). In experimental protocols that use fixed-step adaptation, where the disturbance has a constant component, this confound between the effects of m and A cannot be avoided. Hence, in the main text, we stress the importance of m in our model and we will discuss possible origins and alternative interpretations for such term.

Stimulus convolution. The second term in the RHS of **Equation *A1*** is a convolution of the variable part of the disturbance. For the sinusoidal disturbances used in our datasets, it produces the sinusoidal component of the oculomotor response.

$$h(n+1) = K\sum_{i=1}^{n} p(i)\sin(\omega i)(A-K)^{n-i}. \qquad (A4)$$

The latest experienced stimulus (at trial n) will be fully weighted because $i = n$. Increasing powers of $(A - K)$ will progressively attenuate subsequent older instances of the stimulus until i becomes small enough so that $(A - K)^{n-i}$ becomes negligibly small. This defines a window of trials over which the stimulus contributes in a relevant manner to the oculomotor response. Note that **Equation *A4*** resembles a harmonic components expansion of a pattern with fundamental frequency given by $\omega \sim \frac{1}{T}$, where T is commensurate with the intertrial interval. By design $\omega = \frac{2\pi f}{N}$, where f is the frequency of the stimulus in saccades per block. However, this expansion actually starts populating the spectra of the resulting response by the highest possible harmonic, which in turn is determined by the inter-trial interval T.

Fig A1. Exploration of the 'window of integration'. Weights of the convolution term in **Equation A4** as a function of the trial number for three sets of values of the learning rate $\boldsymbol{K}$ and the persistence rate $\boldsymbol{A}$. As an example, the solid green line depicts the case $\boldsymbol{A} = \mathbf{0.998}$, $\boldsymbol{A} = \mathbf{0.005}$. For those values, it takes more than 300 trials for the weight to decrease to 10% of its full value, suggesting that, if no other process is able to disrupt the accumulation in **Equation A4**, a sizeable number of past trials will influence the response even when only learning from the last error. Depending on the stimulus and the task, this feature may be advantageous or detrimental. The plots also show how strongly higher learning rates and smaller persistence rates result in smaller integration windows. This rigidity in the weighting of the experienced stimulus can be softened by keeping memory of and learning from further errors in the past.

Supplementary Table 1. Generative parameters fitted with the best four models. Model name is shown at the top. The corresponding datasets can be identified by the stimulus frequencies tested: ORIG: 3, 4 and 6cpb. FREQ: 1, 3, 6, 12 and 24cpb.

Supplementary Table 2. ANOVA results on the generative parameters fitted with the best four models. Repeated-measures ANOVA (2 X 3 on data from ORIG; 2 X 5 on data from FREQ) with factors type of adaptation and stimulus frequency was run on each of the four best models. Model name is shown at the side of the table and parameter names are on the top. The dataset is indicated in the cell at the upper left corner next the the parameter names. Highlights indicate the cases where the corresponding factor shows significant effects.

References

1. McLaughlin SC. Parametric adjustment in saccadic eye movements. Perception & Psychophysics. 1967;2: 359–362. doi:10.3758/BF03210071

2. Hopp JJ, Fuchs AF. The characteristics and neuronal substrate of saccadic eye movement plasticity. Prog Neurobiol. 2004;72: 27–53. doi:10.1016/j.pneurobio.2003.12.002

3. Herman JP, Cloud CP, Wallman J. End-point variability is not noise in saccade adaptation. PLoS ONE. 2013;8: e59731. doi:10.1371/journal.pone.0059731.g001

4. Harwood MR, Wallman J. Temporal dynamics and strategy in saccade adaptation. 2004.

5. Collins T, Heed T, Röder B. Eye-movement-driven changes in the perception of auditory space. Atten Percept Psychophys. 2010;72: 736–746. doi:10.3758/APP.72.3.736

6. Azadi R, Harwood MR. Visual cues that are effective for contextual saccade adaptation. Journal of Neurophysiology. 2014;111: 2307–2319. doi:10.1152/jn.00894.2013

7. Chen-Harris H, Joiner WM, Ethier V, Zee DS, Shadmehr R. Adaptive control of saccades via internal feedback. Journal of Neuroscience. 2008;28: 2804–2813. doi:10.1523/JNEUROSCI.5300-07.2008

8. Ethier V, Zee DS, Shadmehr R. Spontaneous recovery of motor memory during saccade adaptation. Journal of Neurophysiology. 2008;99: 2577–2583. doi:10.1152/jn.00015.2008

9. Bridgeman B, Hendry D, Stark L. Failure to detect displacement of the visual world during saccadic eye movements. Vision Research. 1975;15: 719–722.

10. Robinson FR, Noto CT, Bevans SE. Effect of Visual Error Size on Saccade Adaptation in Monkey. Journal of Neurophysiology. American Physiological Society; 2003;90: 1235–1244. doi:10.1152/jn.00656.2002

11. Cassanello CR, Ohl S, Rolfs M. Saccadic adaptation to a systematically varying disturbance. Journal of Neurophysiology. American Physiological Society; 2016;116: 336–350. doi:10.1152/jn.00206.2016

12. Cassanello C, Ohl S, Rolfs M. Saccadic plasticity induced by a periodic disturbance of visual feedback. Journal of Vision. The Association for Research in Vision and Ophthalmology; 2014;14: 740–740. doi:10.1167/14.10.740

13. Hudson TE, Landy MS. Journal of Neuroscience Methods. Journal of Neuroscience Methods. Elsevier B.V; 2012;208: 48–58. doi:10.1016/j.jneumeth.2012.04.001

14. Gray MJ, Blangero A, Herman JP, Wallman J, Harwood MR. Adaptation of naturally paced saccades. Journal of Neurophysiology. 2014;111: 2343–2354. doi:10.1152/jn.00905.2013

15. Baddeley RJ, Ingram HA, Miall RC. System identification applied to a visuomotor task: near-optimal human performance in a noisy changing task. J Neurosci. 2003;23: 3066–3075.

16. Nassar MR, Wilson RC, Heasly B, Gold JI. An approximately Bayesian delta-rule model explains the dynamics of belief updating in a changing environment. Journal of Neuroscience. 2010;30: 12366–12378. doi:10.1523/JNEUROSCI.0822-10.2010

17. Rescorla RA, Wagner AR. A theory of Pavlovian conditioning: Variations in the effectiveness of reinforcement and nonreinforment. Prokasy WF, editor. Classical conditioning II: Current research and theory; 1972.

18. Rolfs M, Knapen T, Cavanagh P. Global saccadic adaptation. Vision Research. Elsevier Ltd; 2010;50: 1882–1890. doi:10.1016/j.visres.2010.06.010

19. Srimal R, Diedrichsen J, Ryklin EB, Curtis CE. Obligatory Adaptation of Saccade Gains. Journal of Neurophysiology. 2008;99: 1554–1558. doi:10.1152/jn.01024.2007

20. Donchin O, Francis JT, Shadmehr R. Quantifying generalization from trial-by-trial behavior of adaptive systems that learn with basis functions: theory and experiments in human motor control. J Neurosci. 2003;23: 9032–9045.

21. Cheng S, Sabes PN. Modeling sensorimotor learning with linear dynamical systems. Neural Computation. 2006;18: 760–793. doi:10.1162/089976606775774651

22. Cheng S, Sabes PN. Calibration of visually guided reaching is driven by error-corrective learning and internal dynamics. Journal of Neurophysiology. American Physiological Society; 2007;97: 3057–3069. doi:10.1152/jn.00897.2006

23. Wörgötter F, Porr B. Temporal sequence learning, prediction, and control: a review of different models and their relation to biological mechanisms. Neural Computation. 2005;17: 245–319. doi:10.1162/0899766053011555

24. Diedrichsen J, Hashambhoy Y, Rane T, Shadmehr R. Neural correlates of reach errors. J Neurosci. 2005;25: 9919–9931. doi:10.1523/JNEUROSCI.1874-05.2005

25. Smith MA, Ghazizadeh A, Shadmehr R. Interacting adaptive processes with different timescales underlie short-term motor learning. PLoS Biol. 2006;4: 1035–1043. doi:10.1371/journal.pbio.0040179

26. Vaswani PA, Shadmehr R. Decay of motor memories in the absence of error. J Neurosci. 2013;33: 7700–7709. doi:10.1523/JNEUROSCI.0124-13.2013

27. Vaswani PA, Shmuelof L, Haith AM, Delnicki RJ, Huang VS, Mazzoni P, et al. Persistent residual errors in motor adaptation tasks: reversion to baseline and exploratory escape. J Neurosci. 2015;35: 6969–6977. doi:10.1523/JNEUROSCI.2656-14.2015

28. Cassanello C, Ostendorf F, Rolfs M. Oculomotor entraining and persistent baseline drift in saccadic adaptation to a sinusoidal disturbance. Journal of Vision. The Association for Research in Vision and Ophthalmology; 2016;16: 379–379. doi:10.1167/16.12.379

29. Cassanello C, Ostendorf F, Rolfs M. State-equation learning model for saccade adaptation. Journal of Vision. The Association for Research in Vision and Ophthalmology; 2017;17: 1142–1142. doi:10.1167/17.10.1142

30. Kass RE, Raftery AE. Bayes factors. Journal of the American Statistical Association. 1995;9: 773–795. doi:10.1080/01621459.1995.10476572

31. Jeffreys H. An Invariant Form for the Prior Probability in Estimation Problems. Proc R Soc Lond A Math Phys Sci. The Royal Society; 1946;186: 453–461. doi:10.2307/97883?ref=no-x-route:2f182c5222c53409df89751cc556fb6f

32. Burge J, Ernst MO, Banks MS. The statistical determinants of adaptation rate in human reaching. Journal of Vision. 2008;8: 20.1–19. doi:10.1167/8.4.20

33. Thoroughman KA, Shadmehr R. Learning of action through adaptive combination of motor primitives. Nature. Nature Publishing Group; 2000;407: 742–747. doi:10.1038/35037588

34. Zarahn E, Weston GD, Liang J, Mazzoni P, Krakauer JW. Explaining savings for visuomotor adaptation: linear time-invariant state-space models are not sufficient. Journal of

Neurophysiology. American Physiological Society; 2008;100: 2537–2548. doi:10.1152/jn.90529.2008

35. Kawato M. Internal models for motor control and trajectory planning. Current Opinion in Neurobiology. 1999;9: 718–727. doi:10.1016/s0959-4388(99)00028-8

36. Wolpert DM, Miall RC, Kawato M. Internal models in the cerebellum. Trends Cogn Sci (Regul Ed). 1998;2: 338–347. doi:10.1016/S1364-6613(98)01221-2

37. Jordan MI, Rumelhart DE. Forward Models: Supervised Learning with a Distal Teacher. Cognitive Science. 1992;16: 307–354. doi:10.1207/s15516709cog1603_1

38. van der Kooij K, Brenner E, van Beers RJ, Smeets JBJ. Visuomotor Adaptation: How Forgetting Keeps Us Conservative. PLoS ONE. 2015;10: e0117901. doi:10.1371/journal.pone.0117901

39. Cameron BD, la Malla de C, López-Moliner J. Why do movements drift in the dark? Passive versus active mechanisms of error accumulation. Journal of Neurophysiology. 2015;114: 390–399. doi:10.1152/jn.00032.2015

40. Akaike H. An information criterion (AIC). Math Sci. Math Sci; 1976;14: 5–9.

41. Akaike H. A new look at the Bayes procedure. Biometrika. 1978;65: 53–59. doi:10.1093/biomet/65.1.53

42. Burnham KP, Anderson DR. Multimodel inference: Understanding AIC and BIC in model selection. Sociological Methods and Research. 2004;33: 261–304. doi:10.1177/0049124104268644

43. Bozdogan H. Model selection and Akaike's Information Criterion (AIC): The general theory and its analytical extensions. Psychometrika. Second Edition. Springer-Verlag; 1987;52: 345–370. doi:10.1007/BF02294361

44. Proakis JG, Manolakis DG. Digital Signal Processing. 2007.

45. Schwarz G. Estimating the dimension of a model. Ann Statist. Institute of Mathematical Statistics; 1978;6: 461–464. doi:10.2307/2958889?ref=search-gateway:b77d54fcff1a48c3e08bcd0ba4ebc395

46. Pelisson D, Alahyane N, Panouillères M, Tilikete C. Sensorimotor adaptation of saccadic eye movements. Neurosci Biobehav Rev. 2010;34: 1103–1120. doi:10.1016/j.neubiorev.2009.12.010

47. Baddeley RJ, Ingram HA, Miall RC. System identification applied to a visuomotor task: near-optimal human performance in a noisy changing task. J Neurosci. 2003;23: 3066–3075.

48. van Beers RJ. How Does Our Motor System Determine Its Learning Rate? PLoS ONE. 2012;7: e49373. doi:10.1371/journal.pone.0049373

49. Shadmehr R, Smith MA, Krakauer JW. Error correction, sensory prediction, and adaptation in motor control. Annu Rev Neurosci. 2010;33: 89–108. doi:10.1146/annurev-neuro-060909-153135

50. Becker W. The neurobiology of saccadic eye movements. Metrics. Reviews of Oculomotor Research. 1989;3: 13–67.

51. Henson DB. Corrective saccades: Effects of altering visual feedback. Vision Research. 1978;18: 63–67. doi:10.1016/0042-6989(78)90078-0

52. Wong AL, Shelhamer M. Sensorimotor adaptation error signals are derived from realistic predictions of movement outcomes. Journal of Neurophysiology. American Physiological Society; 2011;105: 1130–1140. doi:10.1152/jn.00394.2010

53. Collins T, Rolfs M, Deubel H, Cavanagh P. Post-saccadic location judgments reveal remapping of saccade targets to non-foveal locations. Journal of Vision. 2009;9: 29.1–9. doi:10.1167/9.5.29

54. Golla H, Tziridis K, Haarmeier T, Catz N, Barash S, Thier P. Reduced saccadic resilience and impaired saccadic adaptation due to cerebellar disease. Eur J Neurosci. 2008;27: 132–144. doi:10.1111/j.1460-9568.2007.05996.x

55. Miall RC, Weir DJ, Wolpert DM, Stein JF. Is the cerebellum a smith predictor? J Mot Behav. 1993;25: 203–216. doi:10.1080/00222895.1993.9942050

56. Miall RC, Wolpert DM. Forward models for physiological motor control. Neural Networks. 1996;9: 1265–1279. doi:10.1016/S0893-6080(96)00035-4

57. Miall RC, Wolpert DM. The Cerebellum as a Predictive Model of the Motor System: A Smith Predictor Hypothesis. Neural Control of Movement. Boston, MA: Springer, Boston, MA; 1995. pp. 215–223. doi:10.1007/978-1-4615-1985-0_27

58. Chaisanguanthum KS, Shen HH, Sabes PN. Motor variability arises from a slow random walk in neural state. J Neurosci. 2014;34: 12071–12080. doi:10.1523/JNEUROSCI.3001-13.2014

59. Kojima Y, Iwamoto Y, Yoshida K. Memory of Learning Facilitates Saccadic Adaptation in the Monkey. J Neurosci. 2004;24: 7531–7539. doi:10.1523/JNEUROSCI.1741-04.2004

60. Herzfeld DJ, Vaswani PA, Marko MK, Shadmehr R. A memory of errors in sensorimotor learning. Science. 2014;345: 1349–1353. doi:10.1126/science.1253138

61. Körding KP, Tenenbaum JB, Shadmehr R. The dynamics of memory as a consequence of optimal adaptation to a changing body. Nat Neurosci. 2007;10: 779–786. doi:10.1038/nn1901

62. Robinson FR, Soetedjo R, Noto C. Distinct Short-Term and Long-Term Adaptation to Reduce Saccade Size in Monkey. Journal of Neurophysiology. 2006;96: 1030–1041. doi:10.1152/jn.01151.2005

63. Havermann K, Lappe M. The influence of the consistency of postsaccadic visual errors on saccadic adaptation. Journal of Neurophysiology. 2010;103: 3302–3310. doi:10.1152/jn.00970.2009

64. Gonzalez Castro LN, Hadjiosif AM, Hemphill MA, Smith MA. Environmental consistency determines the rate of motor adaptation. Curr Biol. 2014;24: 1050–1061. doi:10.1016/j.cub.2014.03.049

65. Wong AL, Shelhamer M. Saccade adaptation improves in response to a gradually introduced stimulus perturbation. Neurosci Lett. 2011;500: 207–211. doi:10.1016/j.neulet.2011.06.039

66. Huberdeau DM, Krakauer JW, Haith AM. Dual-process decomposition in human sensorimotor adaptation. Current Opinion in Neurobiology. 2015;33: 71–77. doi:10.1016/j.conb.2015.03.003

1228 67. Huang VS, Haith A, Mazzoni P, Krakauer JW. Rethinking Motor Learning and Savings in
1229 Adaptation Paradigms: Model-Free Memory for Successful Actions Combines with Internal
1230 Models. Neuron. 2011;70: 787–801. doi:10.1016/j.neuron.2011.04.012

1231 68. Mazzoni P, Krakauer JW. An implicit plan overrides an explicit strategy during visuomotor
1232 adaptation. J Neurosci. 2006;26: 3642–3645. doi:10.1523/JNEUROSCI.5317-05.2006

1233 69. Haith AM, Krakauer JW. Model-Based and Model-Free Mechanisms of Human Motor
1234 Learning. Advances in Experimental Medicine and Biology. 2013. pp. 1–21.
1235 doi:10.1007/978-1-4614-5465-6_1

1236 70. Criscimagna-Hemminger SE, Bastian AJ, Shadmehr R. Size of Error Affects Cerebellar
1237 Contributions to Motor Learning. Journal of Neurophysiology. 2010;103: 2275–2284.
1238 doi:10.1152/jn.00822.2009

1239 71. Xu-Wilson M, Chen-Harris H, Zee DS, Shadmehr R. Cerebellar Contributions to Adaptive
1240 Control of Saccades in Humans. Journal of Neuroscience. 2009;29: 12930–12939.
1241 doi:10.1523/jneurosci.3115-09.2009

1242 72. Kojima Y, Soetedjo R. Elimination of the error signal in the superior colliculus impairs
1243 saccade motor learning. Proc Natl Acad Sci USA. National Academy of Sciences; 2018;115:
1244 E8987–E8995. doi:10.1073/pnas.1806215115

1245 73. Dash S, Thier P. Cerebellum-Dependent Motor Learning: Lessons from Adaptation of Eye
1246 Movements in Primates. Prog Brain Res. Elsevier; 2014;210: 121–155. doi:10.1016/B978-0-
1247 444-63356-9.00006-6

1248 74. Ritz H, Nassar MR, Frank MJ, Shenhav A. A Control Theoretic Model of Adaptive Learning
1249 in Dynamic Environments. J Cogn Neurosci. 2018;: 1–17. doi:10.1162/jocn_a_01289

1250 75. Rigoux L, Guigon E. A Model of Reward- and Effort-Based Optimal Decision Making and
1251 Motor Control. PLoS Comput Biol. 2012;8. doi:10.1371/journal.pcbi.1002716

1252 76. Thakkar KN, Diwadkar VA, Rolfs M. Oculomotor Prediction: A Window into the Psychotic
1253 Mind. Trends Cogn Sci (Regul Ed). 2017;21: 344–356. doi:10.1016/j.tics.2017.02.001

1254 77. Rösler L, Rolfs M, van der Stigchel S, Neggers SFW, Cahn W, Kahn RS, et al. Failure to
1255 use corollary discharge to remap visual target locations is associated with psychotic
1256 symptom severity in schizophrenia. Journal of Neurophysiology. American Physiological
1257 Society; 2015;114: 1129–1136. doi:10.1152/jn.00155.2015

1258 78. Muhammed K, Manohar S, Ben Yehuda M, Chong TTJ, Tofaris G, Lennox G, et al. Reward
1259 sensitivity deficits modulated by dopamine are associated with apathy in Parkinson's
1260 disease. Brain. 2016;139: 2706–2721. doi:10.1093/brain/aww188

1261 79. Manohar SG, Chong TTJ, Apps MAJ, Batla A, Stamelou M, Jarman PR, et al. Reward Pays
1262 the Cost of Noise Reduction in Motor and Cognitive Control. Curr Biol. 2015;25: 1707–1716.
1263 doi:10.1016/j.cub.2015.05.038

1264 80. Heinzle J, Aponte EA, Stephan KE. Computational models of eye movements and their
1265 application to schizophrenia. Current Opinion in Behavioral Sciences. 2016;11: 21–29.
1266 doi:10.1016/j.cobeha.2016.03.008

1267

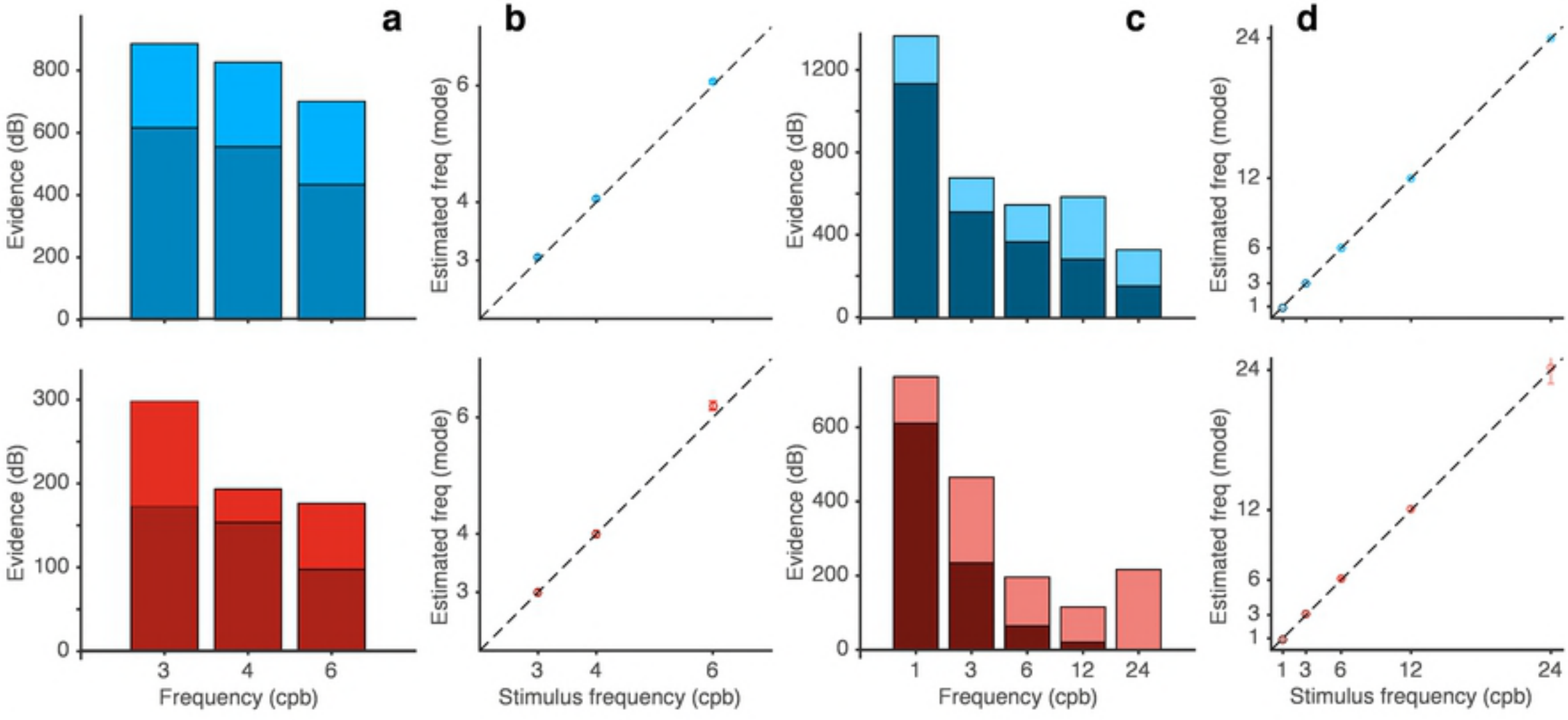
a
b
c
d
Evidence (dB)
Estimated freq (mode)
Frequency (cpb)
Stimulus frequency (cpb)

Figure

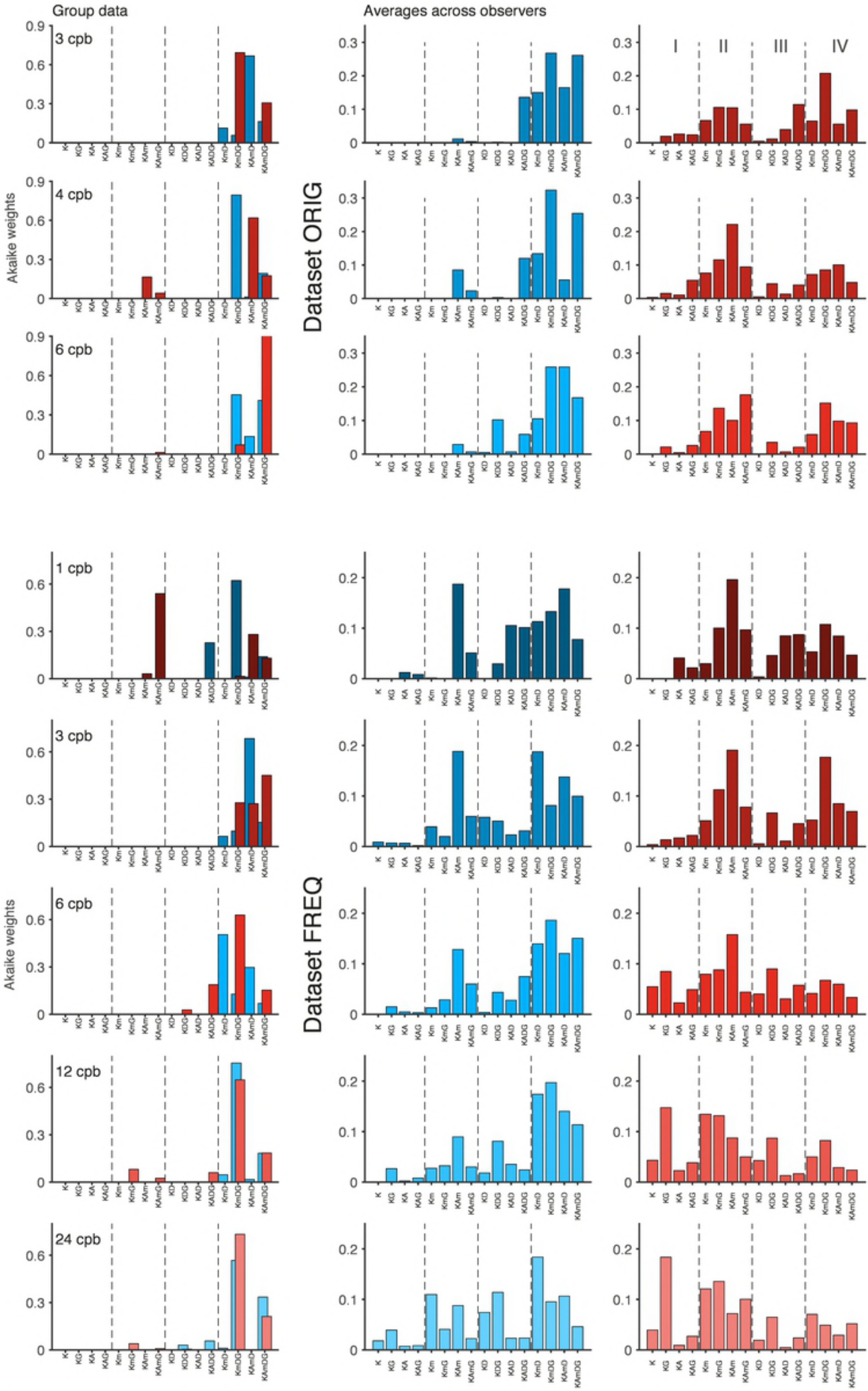
Group data
Averages across observers
Dataset ORIG
Dataset FREQ
Akaike weights
Akaike weights
3 cpb
4 cpb
6 cpb
1 cpb
3 cpb
6 cpb
12 cpb
24 cpb
I
II
III
IV
K
KG
KA
KAG
Km
KmG
KAm
KAmG
KD
KDG
KAD
KADG
KmD
KmDG
KAmD
KAmDG

Figure

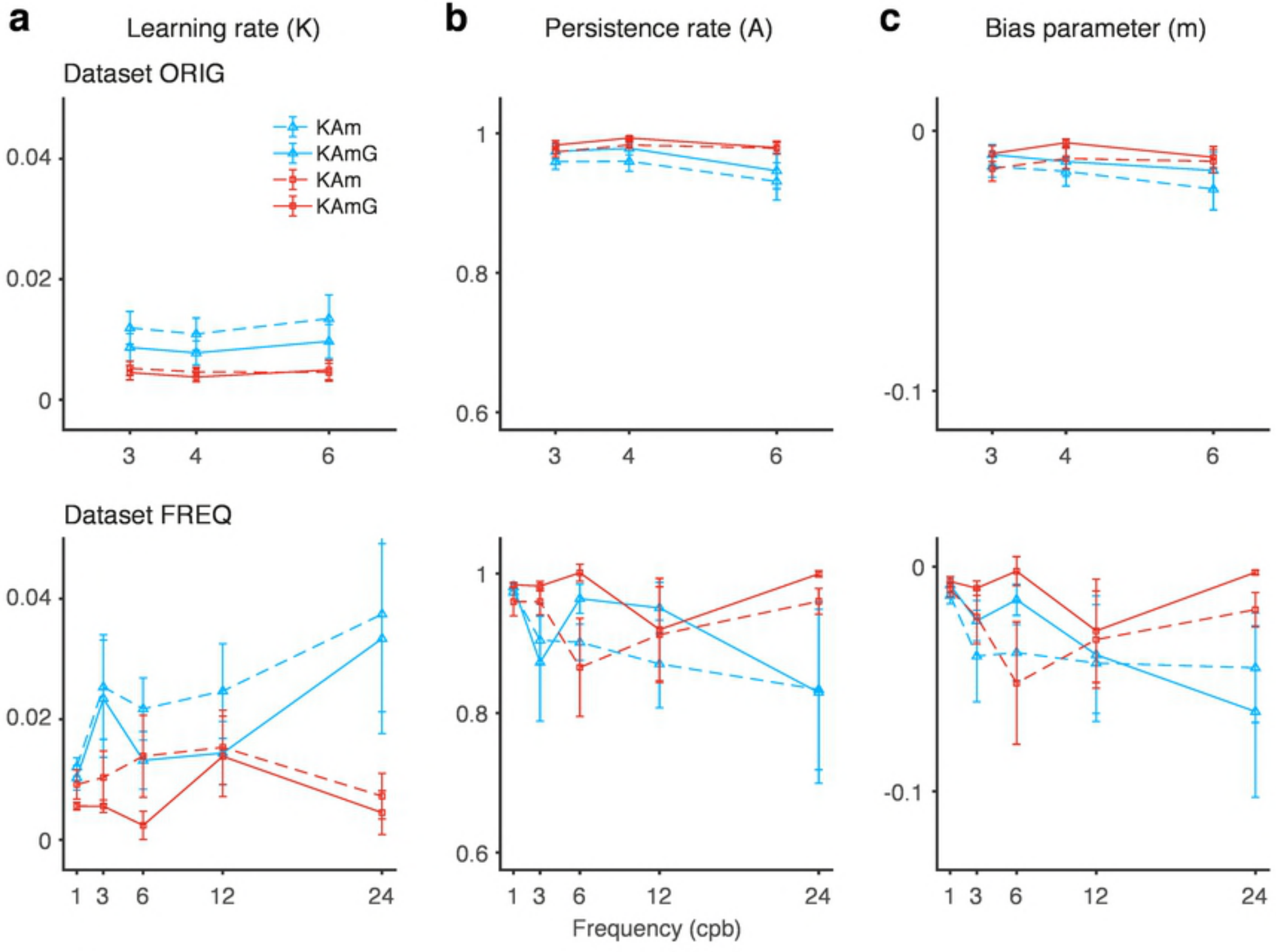
a
Learning rate (K)
b
Persistence rate (A)
c
Bias parameter (m)
Dataset ORIG
KAm
KAmG
KAm
KAmG
0.04
0.02
0
1
0.8
0.6
0
-0.1
3
4
6
Dataset FREQ
1
3
6
12
24
Frequency (cpb)

Figure

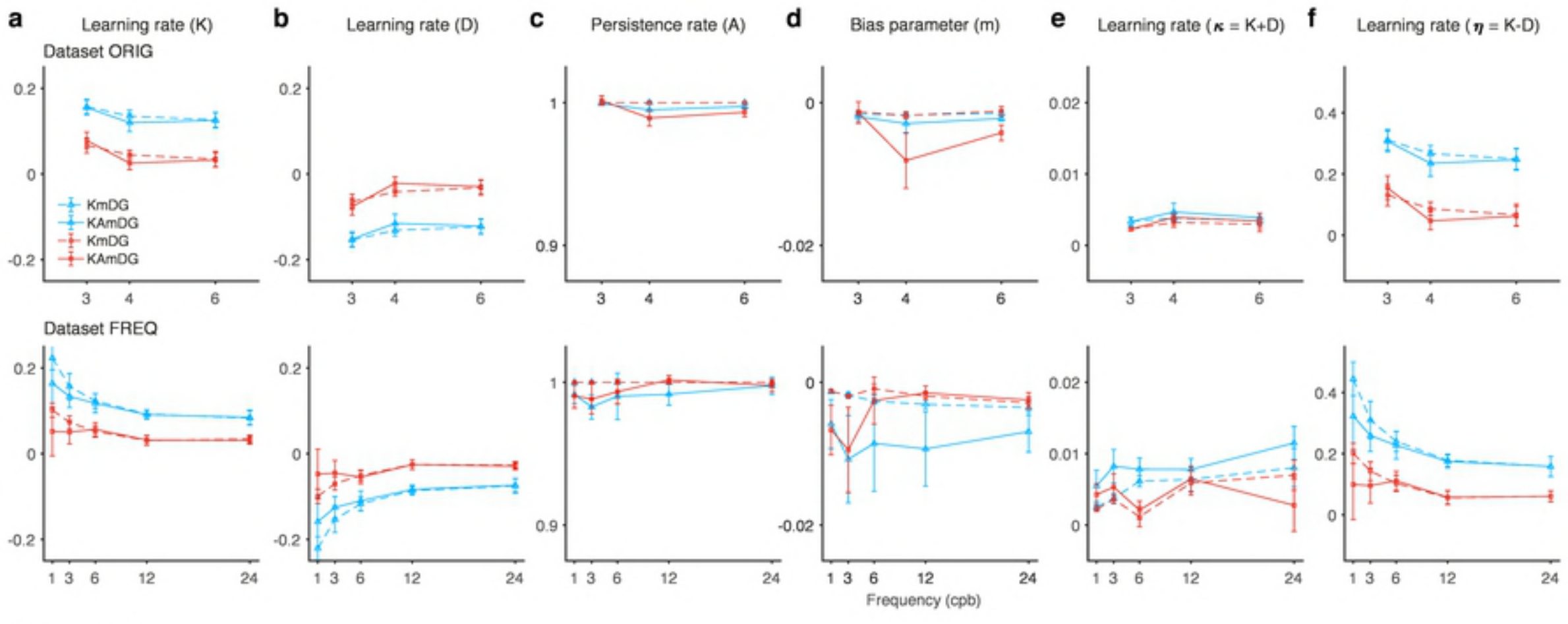
a
Learning rate (K)
b
Learning rate (D)
c
Persistence rate (A)
d
Bias parameter (m)
e
Learning rate (κ = K+D)
f
Learning rate (η = K-D)
Dataset ORIG
Dataset FREQ
KmDG
KAmDG
KmDG
KAmDG
Frequency (cpb)

Figure

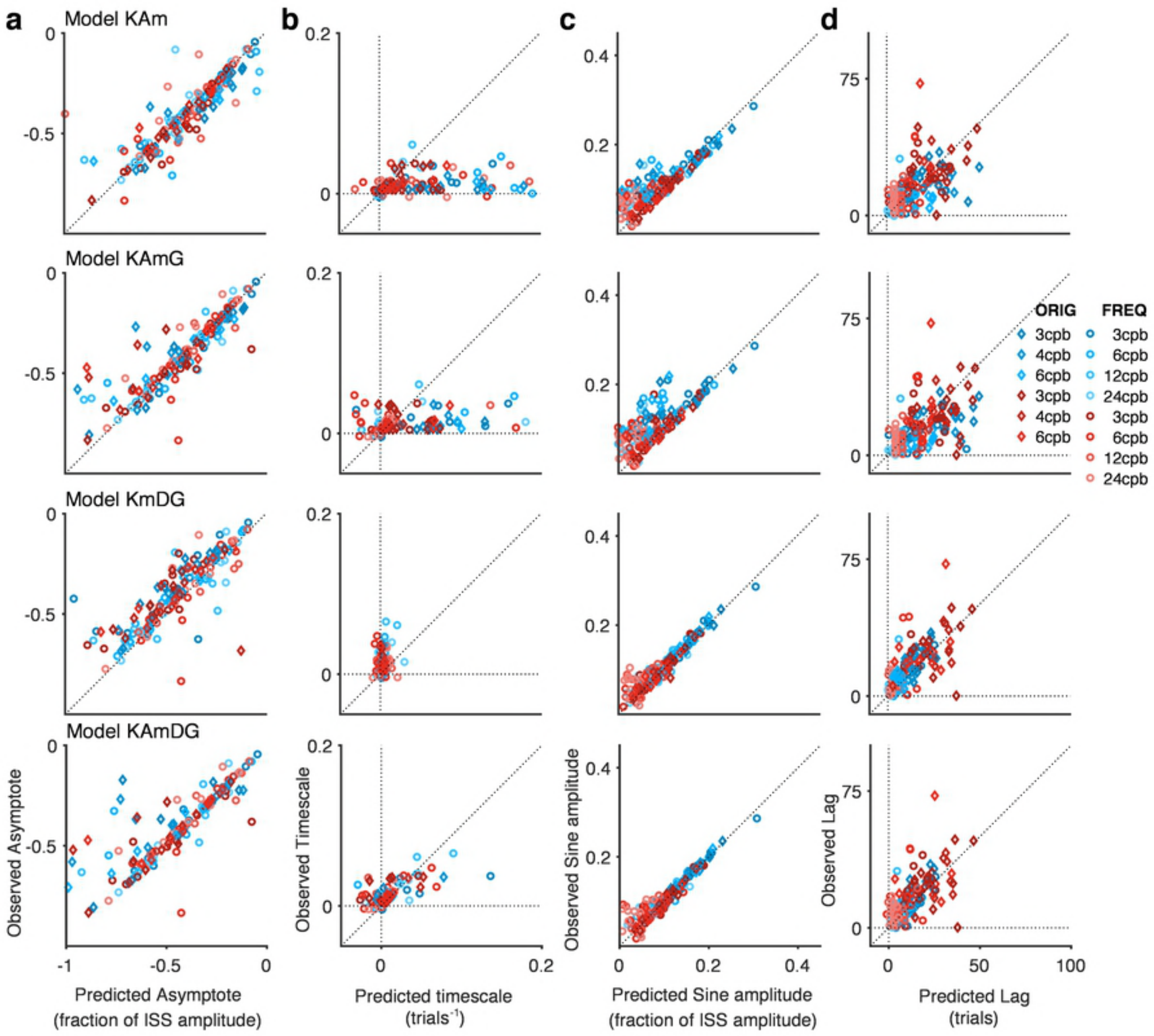
a
b
c
d
Model KAm
Model KAmG
Model KmDG
Model KAmDG
ORIG
FREQ
3cpb
4cpb
6cpb
3cpb
4cpb
6cpb
3cpb
6cpb
12cpb
24cpb
3cpb
6cpb
12cpb
24cpb
Observed Asymptote
Predicted Asymptote
(fraction of ISS amplitude)
Observed Timescale
Predicted timescale
(trials^{-1})
Observed Sine amplitude
Predicted Sine amplitude
(fraction of ISS amplitude)
Observed Lag
Predicted Lag
(trials)

Figure

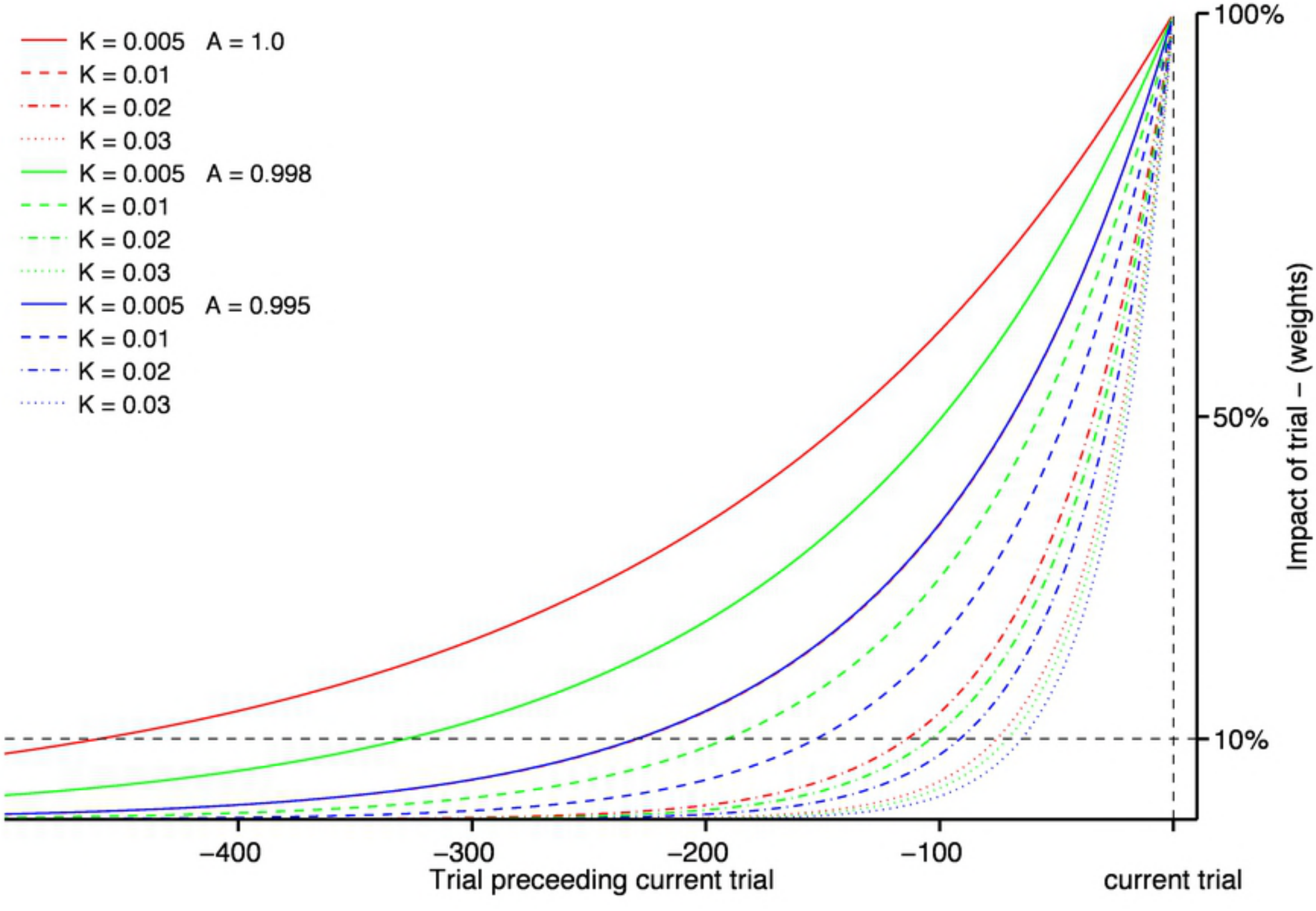
K = 0.005 A = 1.0
K = 0.01
K = 0.02
K = 0.03
K = 0.005 A = 0.998
K = 0.01
K = 0.02
K = 0.03
K = 0.005 A = 0.995
K = 0.01
K = 0.02
K = 0.03
100%
50%
10%
Impact of trial – (weights)
–400
–300
–200
–100
Trial preceeding current trial
current trial

Figure

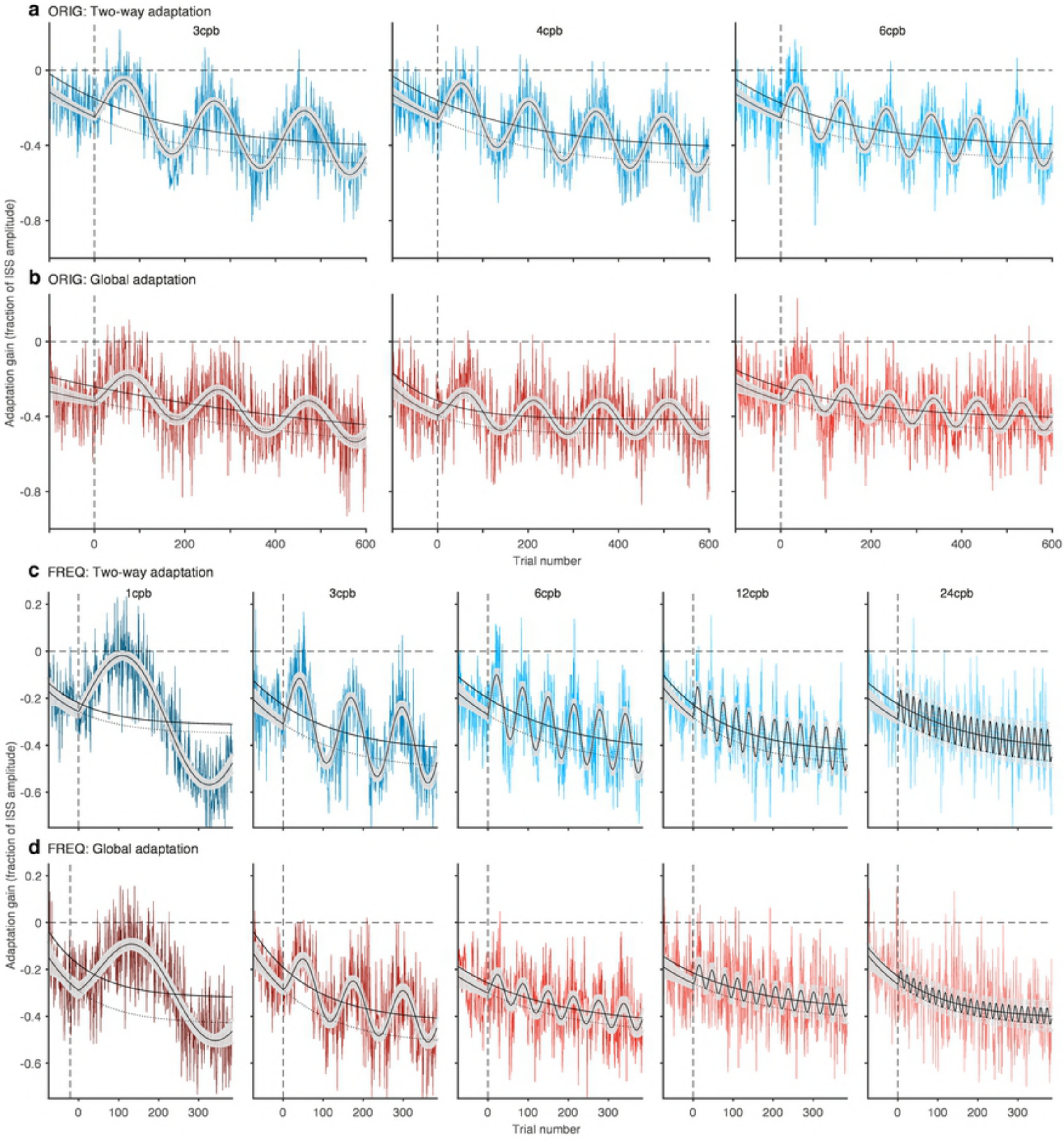
a ORIG: Two-way adaptation
3cpb
4cpb
6cpb
b ORIG: Global adaptation
Adaptation gain (fraction of ISS amplitude)
Trial number
c FREQ: Two-way adaptation
1cpb
3cpb
6cpb
12cpb
24cpb
d FREQ: Global adaptation
Adaptation gain (fraction of ISS amplitude)
Trial number

Figure

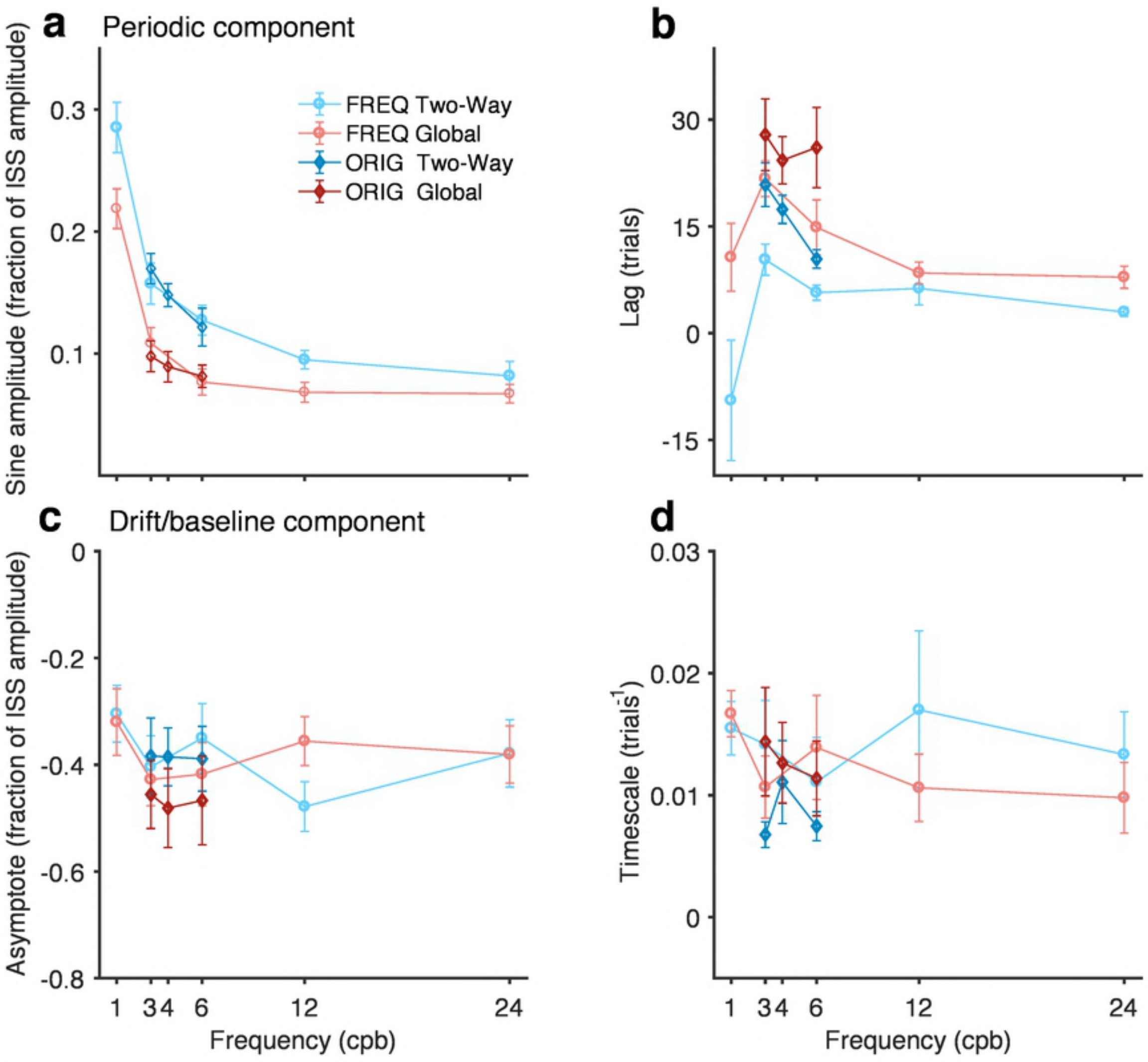
a
Periodic component
Sine amplitude (fraction of ISS amplitude)
0.3
0.2
0.1
FREQ Two-Way
FREQ Global
ORIG Two-Way
ORIG Global
b
Lag (trials)
30
15
0
-15
c
Drift/baseline component
Asymptote (fraction of ISS amplitude)
0
-0.2
-0.4
-0.6
-0.8
1
3
4
6
12
24
Frequency (cpb)
d
Timescale (trials^{-1})
0.03
0.02
0.01
0
1
3
4
6
12
24
Frequency (cpb)

Figure

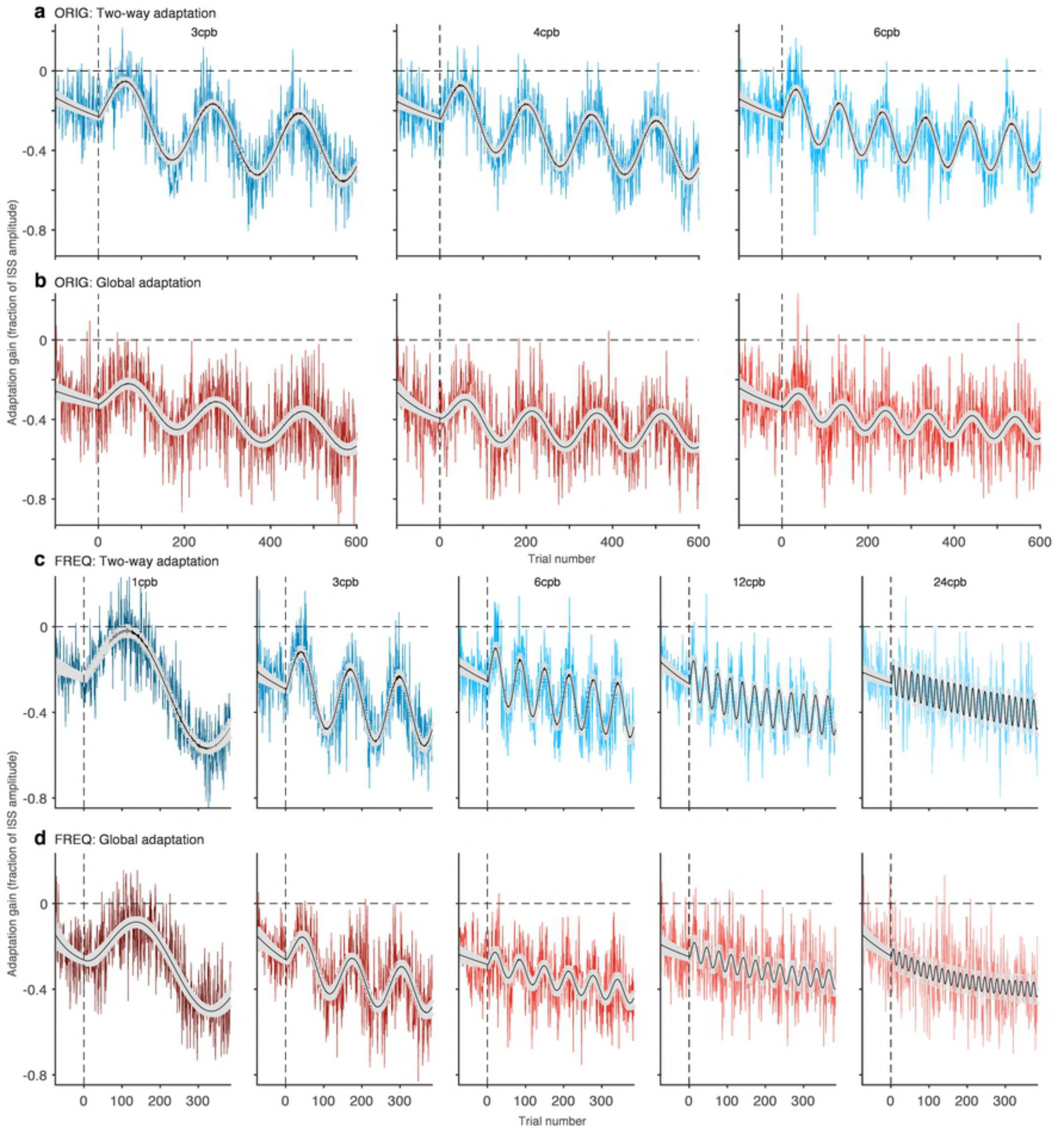
a ORIG: Two-way adaptation
3cpb
4cpb
6cpb
b ORIG: Global adaptation
c FREQ: Two-way adaptation
1cpb
3cpb
6cpb
12cpb
24cpb
d FREQ: Global adaptation
Adaptation gain (fraction of ISS amplitude)
Trial number
0
-0.4
-0.8
0
200
400
600
100
300

Figure